Testing and Modeling of Photo-electric Modulators

by

Matthew J. Weaver

Submitted to the Department of Physics
in partial fulfillment of the requirements for the degree of

Bachelor of Science in Physics

at the

MASSACHUSETTS INSTITUTE OF TECHNOLOGY

June 2012

Author .....
Department of Physics
May 11, 2012

Certified by .....
Rajeev Ram
Professor of Electrical Engineering and Computer Science
Thesis Supervisor

Certified by .....
Erich Ippen
Professor of Physics
Thesis Supervisor

Accepted by .....
Professor Nergis Mavalvala
Senior Thesis Coordinator, Department of Physics

Testing and Modeling of Photo-electric Modulators

by

Matthew J. Weaver

Submitted to the Department of Physics
on May 11, 2012, in partial fulfillment of the
requirements for the degree of
Bachelor of Science in Physics

Abstract

Optical links are a promising alternative to the electrical interconnects that are currently used between chips within a computer. A crucial part of an optical link is a modulator, a device that converts an electrical signal into an optical signal. This thesis explores the physics of how these modulators operate. I built a general purpose optical and electrical testing station to perform these measurements. The optical transmission spectra of the set of modulators studied had extinction ratios in the range of 5 to 27 dB, which is sufficient for modulation. I developed analytical and T-Matrix models to extract physical parameters from the transmission scans, such as light transmission, loss in the ring, and index of refraction of the contact section. The modulators worked with an open eye up to frequencies of 600 MHz. A theoretical model was developed to match the data and experiment with injection and recombination dynamics. Finally, several design solutions are suggested to further improve the modulators and to move towards the goal of modulators that operate at 5 Gb/s.

Thesis Supervisor: Rajeev Ram
Title: Professor of Electrical Engineering and Computer Science

Thesis Supervisor: Erich Ippen
Title: Professor of Physics

Acknowledgments

Working in the Physical Optics and Electronics Group has been an amazing research experience. I would like to thank Professor Ram for leading this group and providing insightful feedback on the research I was performing in lab. He guided me through the entire process of narrowing down my topic and developing a coherent set of experiments. Discussions with him have helped me to understand what I am studying at a much deeper level. I also would like to thank all of the other members of the group for the suggestions they have given me about problems in my research and for all the knowledge they have passed on about a wide range of topics from cell growth to thermodynamics.

Finally I would like to thank Jason Orcutt, my graduate student mentor for this project. He spent many hours patiently explaining concepts to me and showing me how equipment works in lab. Many of the experiments discussed in this thesis were done together with Jason. I have had many great conversations with him about how to proceed with my experiments and about life in general. I would also like to thank friends and family for supporting me throughout my time here at MIT. Overall, working on this project has been a great chance to advance personally and as a physicist.

Contents

List of Figures

List of Tables

Chapter 1

Introduction

This thesis presents experimental measurements and models for a set of electro-optic modulators. In the first chapter I present the reasons for integrating modulators into the CMOS process. I then describe modulators from other groups and the general physics of the operation of modulators. Finally I explain the characteristics of the particular modulators I have been analyzing.

1.1 The Chip Connection Challenge and the CMOS Process

Computers have been improving following Moore's law, which states that the number of transistors doubles approximately every two years. However, as more and more transistors are put onto each chip, the challenge of connecting the chips efficiently is becoming more of an issue [1, 2]. The electrical interconnects that are currently used to connect chips do not have a high enough rate of data transfer and produce a large amount of heat. In order for computers to continue advancing in efficiency and processing power a solution must be found for these problems.

One solution is to use optical interconnects between the chips. An optical fiber is more efficient than an electrical interconnect, because there are no large electrical contacts to charge up. Another advantage of optical fibers is that different signals

can simultaneously be sent through the fiber at different wavelengths using a process called wavelength division multiplexing (WDM). These two advantages would significantly increase processing power and efficiency if optical links were integrated into the connecting chips [1].

An optical link converts electrical signals on one chip into optical signals, sends the signals through a fiber, and then converts the optical signals on another chip back into electrical signals (Figure 1-1.) This necessitates inputing laser light into a waveguide. Light is reflected from a fiber into the waveguide using couplers. The light then travels through the chip in a waveguide, a structure that uses index confinement to channel light. The first active component in the optical link is the electro-optic modulator. This device takes an electric signal and uses it to change the optical power in the waveguide. The physics of these modulators is the subject of this thesis. The light from the modulator couples off chip into a fiber and then couples into a waveguide on another chip. The second active component is the photodetector. This device converts the incoming optical signal back to an electrical signal and completes the optical link.

An optical link must meet certain standards for it to be a suitable substitution for the current electrical interconnects [2]. Overall, the three main constraints on the optical link are speed, power and space. The target speed for the optical link is 96 Tb/s and the target power is 10 W [3]. However, the optical link consists of many different channels, splitting the data rate. Each channel must interface with the electronic circuitry, so the target rate for each channel is about 10 Gb/s, because going significantly faster than the clock rate would require complicated rate changing circuits [4]. Dividing the data rate by power gives a target of about 0.1 pJ/bit. The goal for this set of modulators is to have at least a 10 dB extinction ratio at a rate of 10 Gb/s. The extinction ratio gives the difference between a 1 and a 0 state. It must be large enough that the values are not confused with each other.

In order for the optics to be fully integrated with the chips, they must be fabricated using the same process used to make chips. Computer chips are currently made in a highly sophisticated semiconductor process (CMOS.) This process enables billions

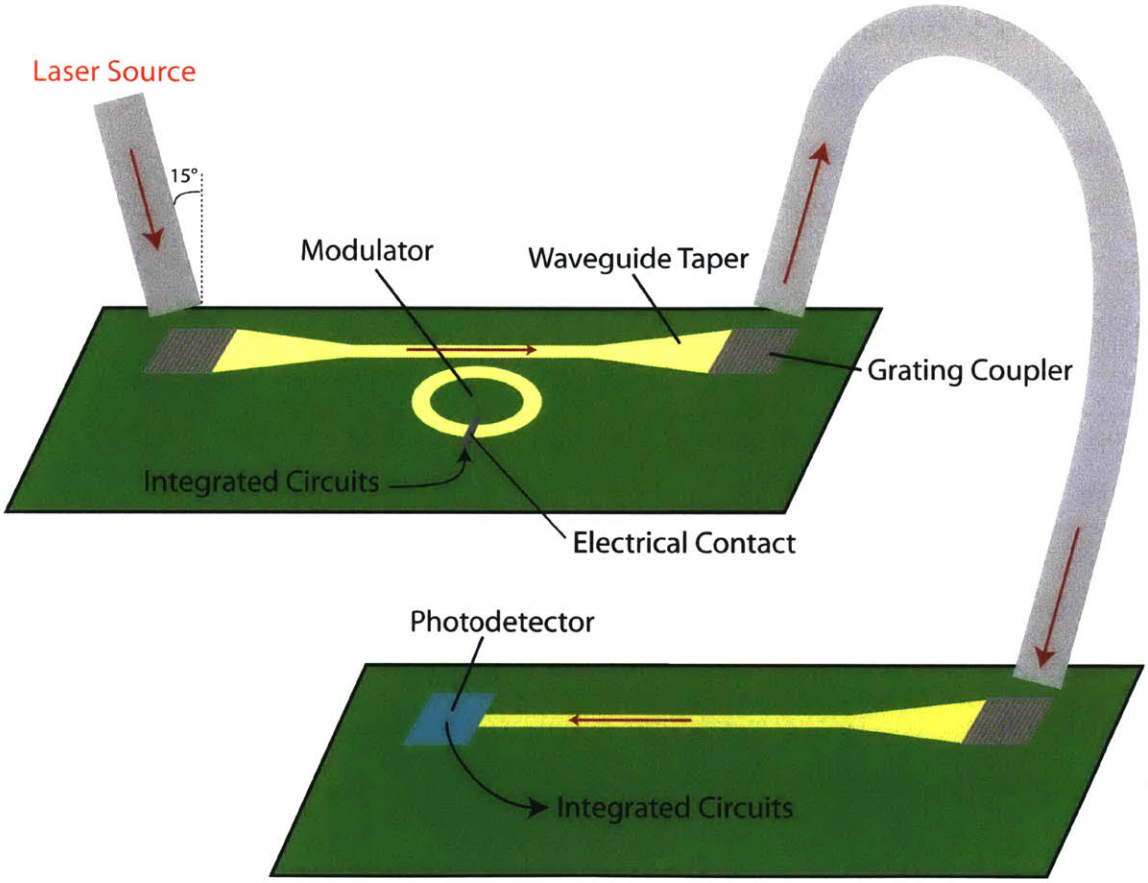

Figure 1-1: The fundamental elements of an optical link. The red arrows indicate the path of the optical signal and the black arrows indicate the path of the electrical signal.

of nanoscale transistors to be made very efficiently. It requires a strict set of design rules as to what materials can be used and what processing steps occur. The end result would be efficient, easily integrated optical interconnects.

CMOS gives engineers a variety of materials to use for device building. In our designs we use single- and poly-crystalline silicon for the waveguides. Because the silicon crystal structures are different, the optical properties of these materials are different. The two most important properties are refractive index and loss, because together these properties determine how much power will be lost as light propagates through the waveguides on the chips.

As stated above, we use silicon cores surrounded by lower index material to confine the light on the chip in waveguides. The surface of the chip that is close to the waveguides needs to have a low index, so that the mode in the waveguide does not overlap with a high-index area. Two methods can be used to achieve this surface property. The first is to etch through the chip, using XeF_2 gas to clear away the silicon under the chip [5]. The other method is to remove the chips from the underlying silicon substrate and then transfer the chips onto a thin layer of Norland Optical Adhesive, a low index glue. This second method will be discussed in Chapter 2, but a diagram of this substrate transfer process is shown in Figure 1-2. A high level of optical confinement to the waveguide is important, because light that escapes into the surrounding material mostly is lost.

1.2 Overview of Electro-optic Modulators

Electro-optic modulators, the focus of this thesis, form a critical part of the optical link by converting electrical data into optical data. There are many different types of modulators, but three that have been built in silicon are Mach-Zehnder modulators, ring modulators and disk modulators. I primarily studied the ring modulator type, as it is more compact and easier to fit on the chips we are using. However, many fast and low power modulators of all three types have been demonstrated.

I will now discuss several modulators that were made by other research groups

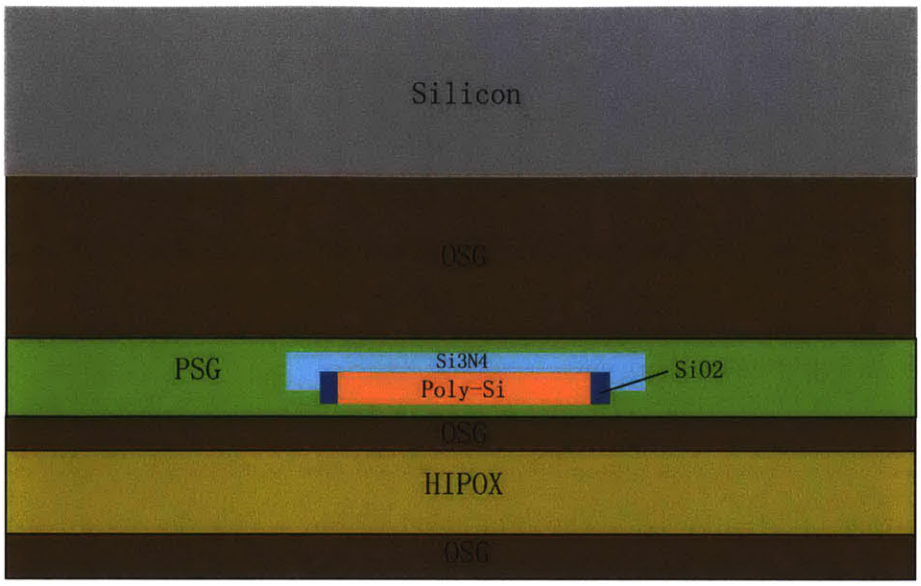

(a)

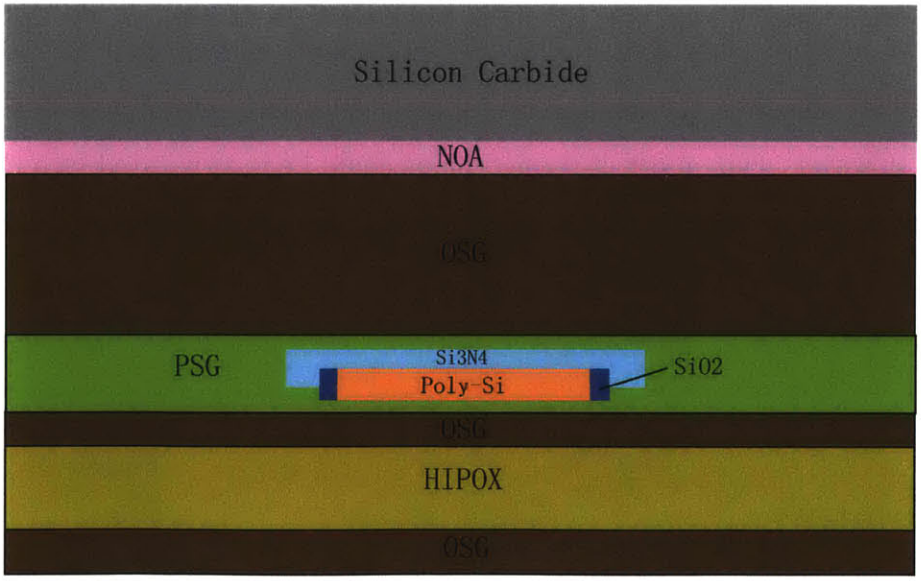

(b)

Figure 1-2: Schematic of the material cross sections of the waveguide in the CMOS process before (1-2a) and after (1-2b) substrate transfer. The materials used are organo-silicate glass (OSG), phosphosilicate glass (PSG), high pressure oxide (HIPOX), silicon nitride, silicon oxide, Norland Optical Adhesive (NOA) and polysilicon. In some designs crystalline silicon is used instead of polysilicon.

Publication	Type	Voltage[V]	Size[μm]	Speed[Gb/s]	Extinction Ratio[dB]
Green[7]	MZ	1.8	100	10	10
Manipatruni[8]	RR	0.15	2.5	1	-
Xu[10]	RR	4	5	12.5	9
Spector[6]	MZ	9	250	26	1
Gunn[11]	RR	-	30	10	20
Watts[12]	DM	1	1.75	12.5	6.8
Zheng[9]	RR	1	15	5	14

Table 1.1: Characteristics of several modulators with different strengths and weaknesses. Mach-Zehnder devices are abreviated as MZ and the size is the length; Ring resonators are abreviated RR and the size is the radius of the ring, and the disc modulator is abbreviated DM.

(Table 1.1). Mach-Zehnder modulators in silicon can operate at 26 Gb/s[6] or with the low power of 51 mW [7]. The limitation of Mach-Zehnder modulators is that they take up more space than rings and discs. Other groups have created efficient ring resonator modulators. One group achieved GHz modulation speed with only 150 mV of peak to peak drive voltage [8] and another group had an efficiency of 400 fJ/bit [9]. Many of the designs can operate at a data rate of 10 Gb/s or higher [10, 11]. However, while most of these designs could be incorporated into the CMOS process, they were not made in a CMOS foundry. In the next section I discuss how ring resonators operate.

1.3 Features and Function of Ring Resonator Modulators

Ring resonator modulators are the type of modulator studied in this thesis. They consist of a straight through waveguide with an adjacent ring waveguide (Figure 1-3). The two waveguides are close enough to each other that they are coupled and light can travel between the two waveguides. The amplitude of the output optical signal changes based upon the interference of the light coupling out of the ring and the light inside the through waveguide. The resonant wavelength inside the ring is changed using an electrical signal. When the resonant wavelength shifts, the interference

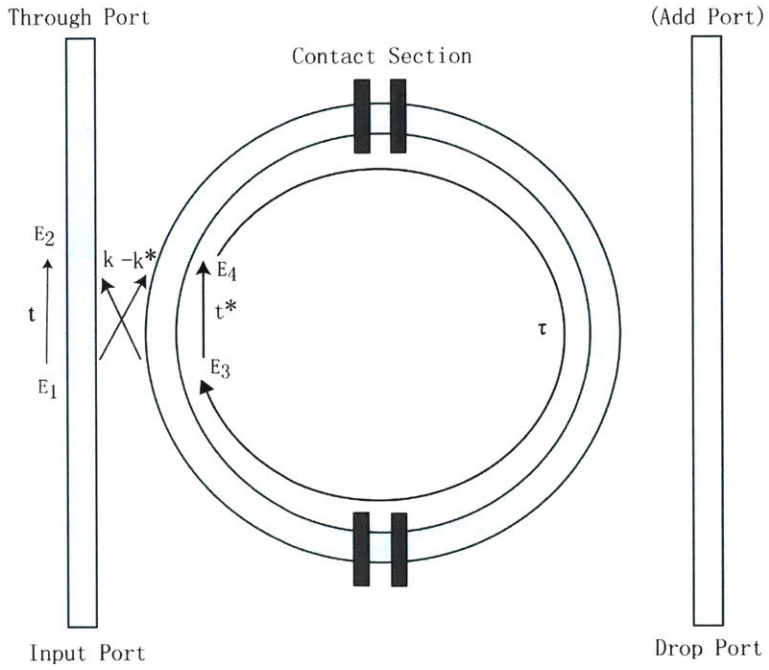

Figure 1-3: The general format of a ring modulator. The waveguide on the right is only included in designs with a drop port. The structure of the contact section also varies depending on the type of modulator.

properties in the through waveguide change and hence the output optical amplitude changes. This process results in an electrical modulation of the optical signal.

There are several parameters related to the structure of the modulator that determine its performance. These parameters are the transmission coefficient t, the ring loss coefficient τ, the free carrier lifetime and the device capacitance. The first two of these parameters determine the static characteristics of the ring, because they indicate the ratio of energy in the ring to energy in the through waveguide. t and τ can be used to calculate the optical transfer, T, of the ring, by using them to determine the relationships between the fields at different points. We start with the following set of equations:

$$\begin{pmatrix} E_2 \\ E_4 \end{pmatrix} = \begin{pmatrix} t & \kappa \\ -\kappa^* & t^* \end{pmatrix} \begin{pmatrix} E_1 \\ E_3 \end{pmatrix} \tag{1.1}$$

$$E_3 = \tau e^{i\phi} E_4 \tag{1.2}$$

κ is the coupling coefficient to the ring. ϕ is the phase factor picked up traveling through the ring, $2\pi L_{eff}/\lambda$, where L_{eff} is the effective index of the waveguide multiplied by the length and λ is the wavelength. By plugging these two equations into each other and using conservation of energy at the junction ($|t|^2 + |\kappa|^2 = 1$), we arrive at the following general transmission equation for modulators [13]:

$$\frac{|E_2|^2}{|E_1|^2} = T = \frac{t^2 - 2t\tau cos\phi + \tau^2}{1 - 2t\tau cos\phi + (t\tau)^2} \tag{1.3}$$

Carrier lifetime and device capacitance determine the high-speed characteristics of the device. It takes time for free carriers to be injected into the waveguide in the ring. This time and the resulting maximum speed of modulation is determined by the length of time that electrons and holes survive in the waveguide and the amount of current that is needed to charge up the p and n regions on either side of the device. I will discuss these parameters and the high speed operation of the modulators in Chapter 4.

These four parameters must be chosen well to have an effective modulator. In particular t and τ must be equal to produce a deep resonance. This is called the critical coupling condition, because matching t and τ produces the deepest resonance [13]. Some of the modulators have thermal tuning that allows the coupling of the modulators to be changed. However, it is still important that the values of t and τ be close together.

The transmission coefficient, t, is the fraction of the light that continues in the waveguide from the input port to the through port (i.e. the light that doesn't couple into the ring.) This parameter is determined by the width of the through waveguide at the interface and the distance between the through waveguide and the ring waveguide. The loss coefficient, τ is determined by the ring waveguide loss and the loss at finger and contact regions.

Some modulators also include a drop waveguide (Figure 1-3). This is another straight waveguide on the other side of the ring waveguide that is coupled to the ring. The drop waveguide has no input optical power, so the only light that comes

out of this waveguide is the light coupled out of the ring. Measuring the power in the drop port is therefore an indirect way of measuring power in the ring. Many of the modulators tested had drop ports for testing purposes. However, because light is coupled out of the ring on both sides, there is more power lost in the ring, and this reduces modulation of the optical signal at the through port. I studied modulators with and without the drop port.

We use injection of current to change the resonant wavelength of the ring waveguide. Metal layers from upper layers of the chip contact to p and n doped silicon next to the waveguide. This forms a pin structure similar to that of a diode. By applying a bias across the pin junction, electrons and holes are injected into the waveguide. The index of refraction of the contact region decreases because of the electro-refractive effect [14]. The index also tends to increase because of the heat in the contact region from resistive power release [14]. Depending on the balance of these two effects, the index of the contact region increases or decreases and the effective length of the ring increases or decreases, respectively. This causes a shift in the resonant wavelength.

1.4 Slab and Rib Modulators

Eugen Zgraggen, a former graduate student in our lab, designed a set of ring resonator modulators that we call slab modulators [15]. These modulators have a straight contact section and a curved coupling section with the other waveguides (Figure 1-4). The curvature of the waveguide in the racetrack is varied such that the light wave can smoothly transition between the curved sections and the straight section of the waveguide. A wider width is used in the contact section, because it causes the light mode to be more confined to the waveguide so there is less leakage through the contacts.

The contacts to the waveguide are highly optimized. Each contact section has two or three contact fingers that are spaced apart in such a way that higher order modes cannot couple between the fingers. They also have been configured to minimize optical loss through the metal regions of the contacts. Furthermore, the length of

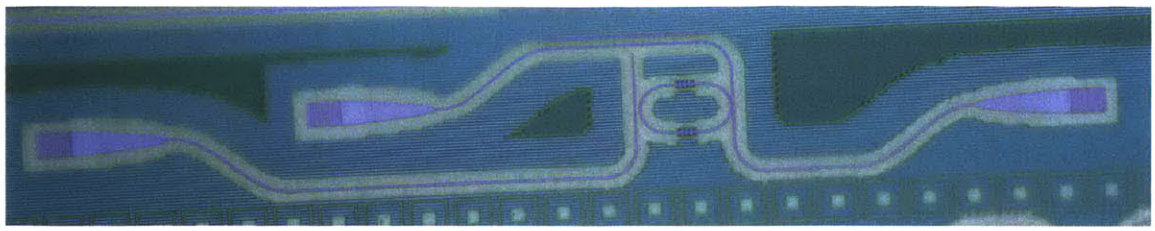

Figure 1-4: Photo of a slab modulator. The contacts are the dark sections on the straight part of the racetrack. This chip has been released from the silicon substrate so that the optics are facing up.

the fingers corresponds to half the wavelength to minimize back reflectance, because light reflected backward off of the front and back edges of the contacts destructively interferes.

Zgraggen simulated these modulators to derive their expected performance. The extinction ratio is the difference in power between an off and an on optical signal. Zgraggen predicted that the extinction ratio would be around 10 dB for the three contact devices and 38 dB for the two contact devices. Another important parameter is the 3 dB bandwidth, which measures the width of the resonance. Zgraggen predicted that the two contact devices would have widths of around 110 GHz (0.6 nm), whereas the two contact devices would have widths of about 1 GHz (0.006 nm). Together these two parameters determine how well the modulator works.

Several chips have been made with Zgraggen's original design. However, the early attempts at incorporating these designs (EOS1 and EOS2) faced high waveguide loss that led to shallow and wide resonances. The best modulator results from the first tape-out with Zgraggen's designs had an extinction ratio of 4 dB and a resonance width of about 2 nm. The resonance is shown in Figure 1-5. I will discuss some of the later versions of these modulators (EOS8 and EOS10) in Chapters 2 and 4, as these were the modulators I focused on in my research.

Another design that is used in our group is the rib waveguide ring modulator. These devices have the same general structure, but the waveguide and contact designs are different. Most of the waveguide is raised up into a rib structure. The p and n doped contact regions are only in the bottom layer, so there is less mode overlap

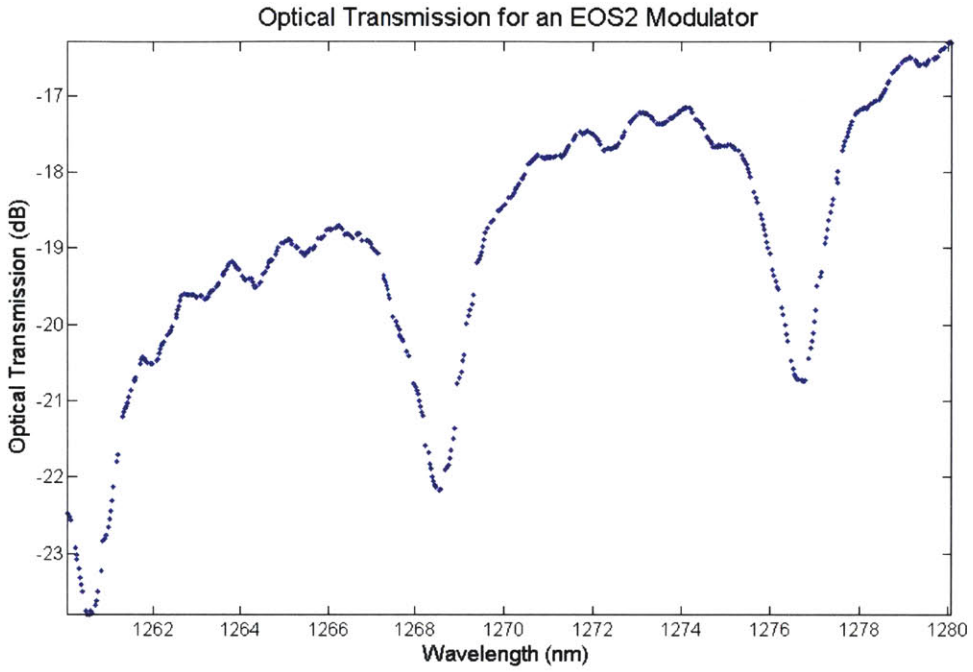

Figure 1-5: Optical transmission from the input port to the drop port of an EOS2 modulator. The wavelength of the input light is varied using a tunable laser. The transmission spectrum shows the resonances of the modulator, but they are neither deep nor narrow. The overall spectrum is most likely slanted due to the wavelength dependence of the fiber couplers.

with the contacts. The contact region is also continuous around most of the ring, not separated into fingers as in Zgraggen's design.

1.5 Thesis Overview

This thesis addresses the physics of electro-optic modulators. Chapter 2 will explain the experimental setup and some of the materials and methods used in preparing samples. Chapter 2 also covers the static optical and electrical data taken from the modulators. Chapter 3 explains three theoretical models I have used to explain the static properties of the modulators: a simple analytical model, a T-matrix multiplication model and Fimmwave simulation models. Chapter 4 discusses the high-speed characteristics of the modulators. This includes the experimental setup used to measure the high speed characteristics, the data taken and a dynamic model that fits the data. Chapter 5 explains improvements that could be made in future runs and more experiments that could be done to better understand the modulators.

Chapter 2

Materials and Methods, Static Data

To study the optical and electrical properties of photonic devices I built a setup to couple laser light onto the chips being analyzed. This capability enabled a variety of measurements of the optical and electrical properties of the modulators. The most indicative static measurements of the modulators are the optical transfer measurement (power vs. wavelength) and the electrical IV measurement. These two measurements provide sufficient criteria to evaluate the different modulators.

In this Chapter I first discuss the photonic testing station and its construction. I then describe the substrate transfer process that is used to expose the photonics to a low index material. I show some of the optical transfer data and some of the electrical measurements for the EOS8 chip. Finally I compare the devices on this tape-out and explain which modulators have the best characteristics.

2.1 Probing and Optical Testing Station

The optical testing station is used to study the optical and electrical characteristics of devices on a CMOS chip. This requires precise control of the light entering and exiting the chip and using probes to electrically contact the chip. Effectively accomplishing these goals also requires precise movement of the fibers and stages of the system. We

have devices designed for 1550 nm and 1280 nm laser light, so the setup must be able to produce and handle these wavelengths of light at low powers in the range of 1 nW to 1 mW. The electrical contacts also must be able to land on pads that are 100 μm wide. All of these requirements are met in the design I built below (Figure 2-1). This design is mostly based upon another setup built by Jason Orcutt [3].

The first important aspect of the experiment is producing the laser light. We use two tunable laser sources: the Santec TSL-210F and the HP 8164A. The Santec has four tunable lasers inside it that enable it to emit light in the 1260 to 1630 nm range. The HP is more stable, but is limited to the 1500 to 1600 nm range. These lasers produce single mode polarized light that passes into a single mode fiber. It is possible to control the output power of the HP and Santec in the range of 1-4 mW and 3-10 mW respectively. Polarization control paddles are used to adjust the polarization to the desired TE or TM mode. Polarization paddles consist of three waveplates, each of which uses birefringence to shift the phase between the light components polarized along two axes. Turning the three paddles enables selection of any polarization. These lasers form the basis for the optical transmission scanning and wavelength control of the optical setup.

Cameras and a microscope are used to see the positioning of the components. The microscope is mounted on two perpendicular rails so that it can move in the plane above the sample. There is an infrared camera attached to the microscope from above. This camera detects the laser light on the chip and connects to a computer where the images are displayed. The infrared camera is useful both because it shows what we cannot see and because it is not safe to look through the microscope when the laser is on. A second camera is positioned behind the chip and displays the vertical positioning of the fibers and chip. Together these three devices give a complete picture of the relative positioning of the fibers, probes and chip.

There are also three stages that move the two fibers and the chip. The fiber stages (Figure 2-2) can move in the x, y, and z directions using voltage-controlled closed-loop piezo stages. The resolution of this movement is 30 nm. There is an additional stage mounted on top to give the fiber the pitch and yaw degrees of freedom. The fiber is

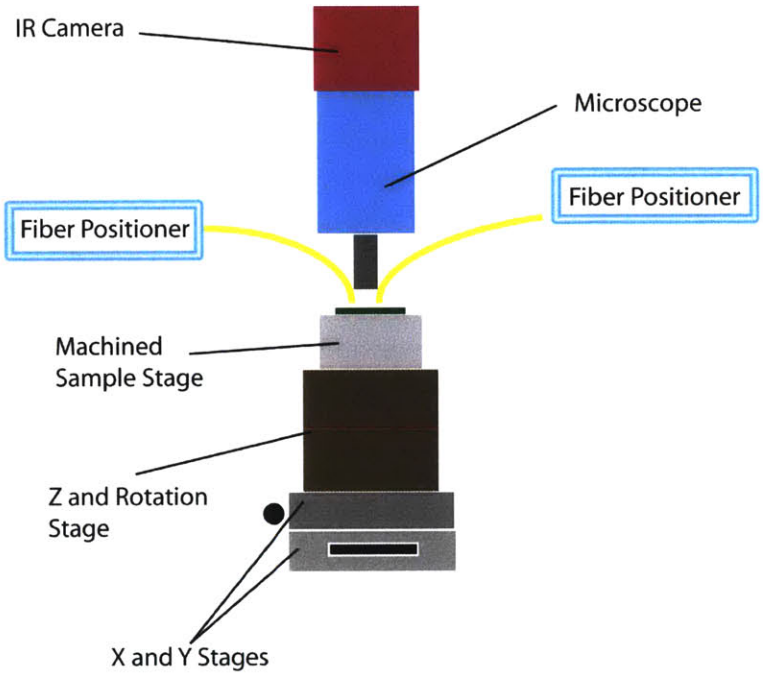

Figure 2-1: A side-view of the setup. The bottom section moves the chip with four degrees of freedom. The top section moves the microscope and displays the IR signal on the computer. The camera is behind the setup, and any electrical contacts are from the front.

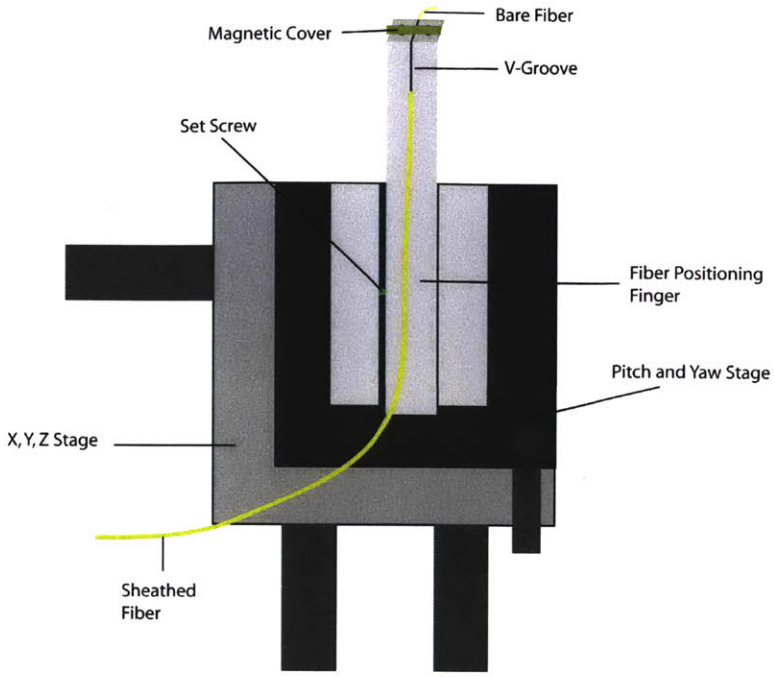

Figure 2-2: A fiber positioner as seen from above. The end of the fiber positioning finger holds the bare fiber at the angle determined by the edge of the finger. The finger is held in place by two metal bars with a set screw. The stages give five degrees of freedom for movement of the fiber with 30 nm resolution in the x, y and z directions.

held in a v-groove on a metal finger, fastened down with a magnet. This finger can slide back and forth on top of the stage and is locked in place with a perpendicular screw. This stage setup enables complete control of the position and orientation of the fiber. Another stage with x,y,z and in-plane rotation control is used for the chip. Control of this stage is coarser, because it only needs to get the chip in approximately the right location. On top of the chip stage there is vacuum piece that holds the chip down.

There are two types of electrical contacting devices. Both have x, y and z control, like the stages. The first type is just a single contacting tip. Two of these are used for the input and ground voltages. However, these probes are only useful at DC or low frequency AC currents. The second type is a GSG probe, which lands on three contacts. This probe has an additional degree of freedom for the rotation that is necessary to land the probe evenly on the chip. This second probe works well at any frequency.

A computer program is used to coordinate the operations. Once the chip and fiber are positioned so that the fibers and on-chip waveguide are coupled, a wavelength scan can be completed. The computer sends a GPIB command to the laser to turn on and switch to a certain wavelength. The light then travels from the laser to the polarization control paddles. The light is then split in a 90-10 splitter, with 10 percent of the light going to an optical power measurement port. The rest of the light then passes through the chip and to another measurement port. The computer calculates the loss based on these two power measurements. The wavelength is incremented and the process is repeated. The computer can also interface with a parameter analyzer when the parameter analyzer is being used to input an electrical signal.

This optical testing setup enables a number of diverse experiments to be performed. The most commonly performed experiment is a simple wavelength transmission scan. The system can also take electrical IV curve measurements and shifts in transmission at a DC voltage. In Chapter 4, I will describe how more instruments can be added to allow high frequency measurements. The testing setup station was crucial for studying the modulators and other photoelectric devices.

2.2 Substrate Transfer Technique

Before chips could be tested in the optical testing station they were properly prepared. The chips from the foundry are mounted on a silicon substrate, and the waveguides in the chip are close enough to the bottom surface that there is significant loss due to the optical mode in the waveguide overlapping with the underlying silicon. Therefore the chip is substrate released, and the chip is mounted on the other side with crystal bond onto silicon, and the original silicon is removed. At this stage the optics face the air and the electronic contacts face down to the crystal bond. Another flip is required so that the optics still face a low index material, but the electrical contacts are accessible for testing.

To complete this substrate transfer Norland Optical Adhesive 71 (NOA) was used. The steps were gradually refined to find the method that produced the best results.

First the sample was cleaned and a square of glass the size of the chip was scribed then broken. The glass square was replaced with a diced square of silicon carbide, because silicon carbide has better heat conduction, so the sample heated up less during electrical testing when silicon carbide was used. The second step was to put a small drop of NOA(almost as small as possible) on the chip then place the silicon carbide square on top of the chip. The layer of NOA was as thin as possible, yet still covered the entire chip. Obtaining the right amount required practice runs with non-valuable samples.

The third step was curing the NOA with exposure to an hour of UV light followed by baking the sample overnight(about 12 hours) on a hot plate at 60°C. The final step was to remove the silicon and crystal bond underneath the chip. Originally the entire chip was soaked in acetone for some time until the crystal bond all dissolved. However, the acetone also attacked the NOA, so this method was not very effective. The current procedure is to place the chip, crystal bond down, on a hot plate at about 85°C until the crystal bond melts. The chip is then pulled off of the silicon, and then the remaining crystal bond is rinsed off with acetone using a dropper and tex wipes. The result is a chip with electronic contacts facing up and a layer of NOA between the optics and the silicon carbide. Once the chip has been transferred it is ready for optical experiments.

2.3 Optical Transfer Characteristics

Many of the optical properties of a modulator can be determined from the optical transmission through the device as a function of wavelength. In order for a modulator to produce an output optical signal, it must have a large range of power output. This range is called the extinction ratio and is often given in units of dB. The power out of the modulator is wavelength dependent due to its resonant nature, so the maximum and minimum power can be determined from a wavelength scan of the optical transmission. The wavelength scan also shows the width of the resonance. Narrow resonances are better, because the resonance can more easily be shifted from

maximum to minimum. I will show some of these wavelength scans and discuss the differences (Figure 2-3).

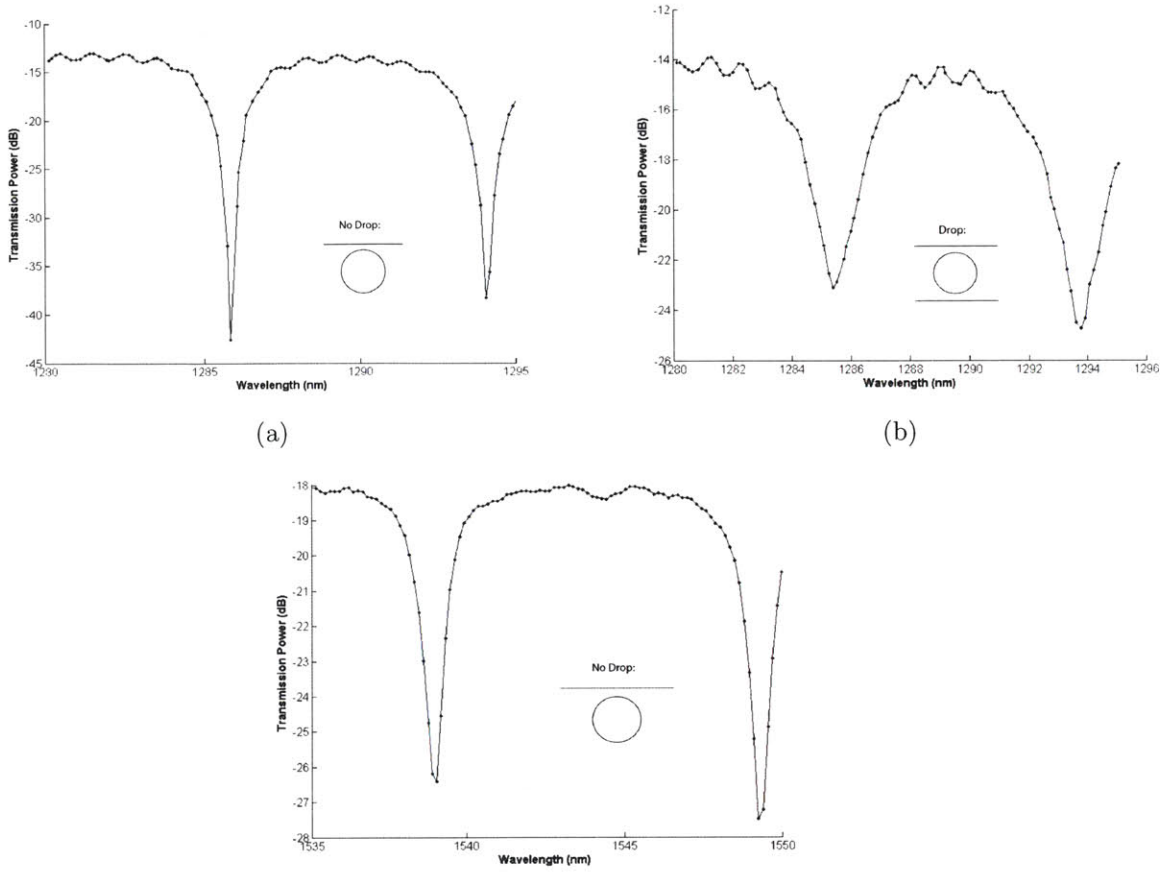

Figure 2-3: Optical transmission measurements for three different modulator devices from the EOS8 run. 2-3a is a 1280 nm modulator with no drop port, 2-3b is a 1280 nm modulator with a drop port and 2-3c is a 1550 nm modulator with no drop port.

A comparison of Figure 2-3a and Figure 2-3b demonstrates some of the differences between the presence and absence of a drop port. The device with the drop port performed worse in both extinction ratio and resonance width. The decrease in both of these parameters is caused by the light that is lost in the ring to the drop port. The 1550 nm modulator in Figure 2-3c most likely had lower extinction ratio as a result of worse coupling of the waveguide to the resonant ring. Further explanation for these differences will be discussed in Chapter 3. The roughly sinusoidal variations

on top of the resonances are caused by a Fabry-Perot reflection. Light is reflected off the input and output grating couplers and forms smaller resonances due to the interference between the output light and the reflected light. These devices are from a more recent run (EOS8) than the modulators in Chapter 1(EOS2). The EOS8 run has waveguides with less loss, so it is not surprising that the optical characteristics are better.

2.4 Electrical Measurements

Another important aspect of the modulator design is how well carriers (electrons and holes) can be injected into the waveguide. This can be judged by taking an IV curve. If a satisfactory current can be acheived at a lower voltage, this means less power is dissipated in the waveguide and the device is less likely to break. Most of the devices in the EOS2 run did not have the current necessary for operation at low voltage. These devices needed about 2 volts to get 1 μA of current. The following set of modulators performed much better.

Most of the devices in the EOS8 run had very similar IV curves to the one shown in Figure 2-4. These devices achieved a μA of current at about 0.78 V and a mA of current at about 1.1 V. In these devices finger contacts to the waveguide were used to inject current. Modulators with 6 fingers had more current than modulators with 4 fingers. Current is necessary to shift the refractive index in the modulators. If not enough current is injected, the resonant wavelength is not shifted enough for modulation. 100 μA to 1mA is the range of current necessary for driving the modulators, and all of the EOS8 devices can reach this level without releasing too much power. The shifted resonance is shown in Figure 2-5, with different current inputs.

2.5 Comparison of Modulators

Table 2.1 indicates the optical properties of the eight modulators studied. In all cases devices without drop ports had better extinction and resonance width than

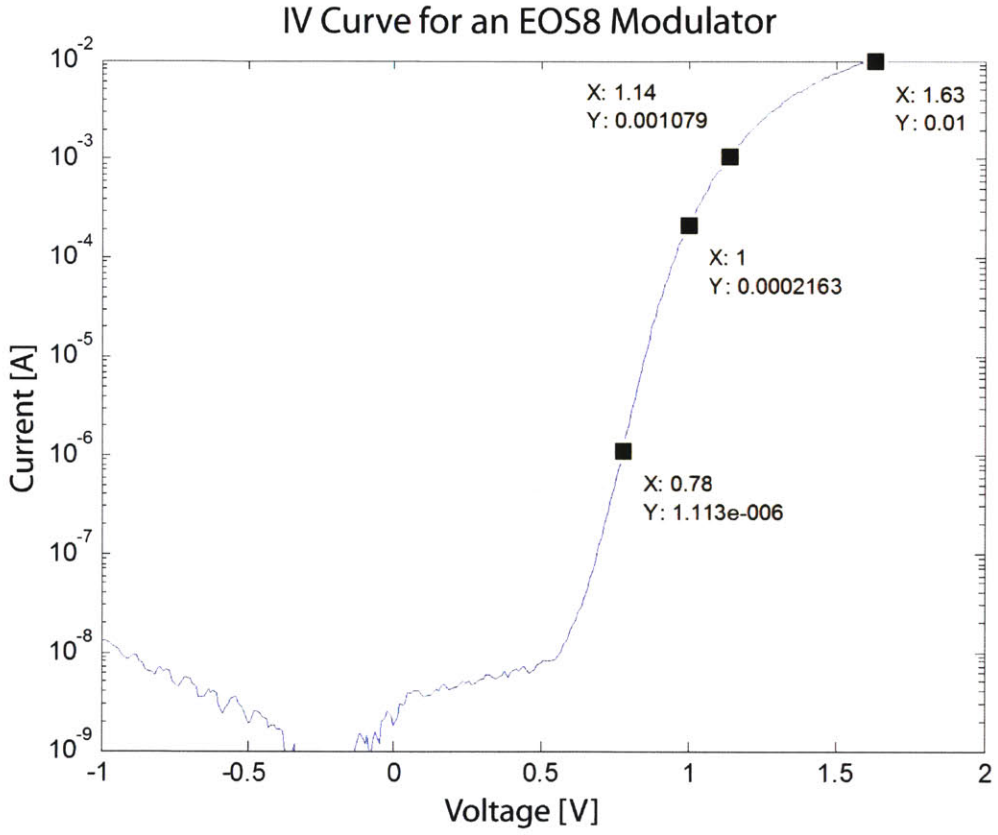

Figure 2-4: This is an IV curve of one of the modulators. The significance of this data is that it shows how much power is necessary to input the current for shifting the resonance of the modulator.

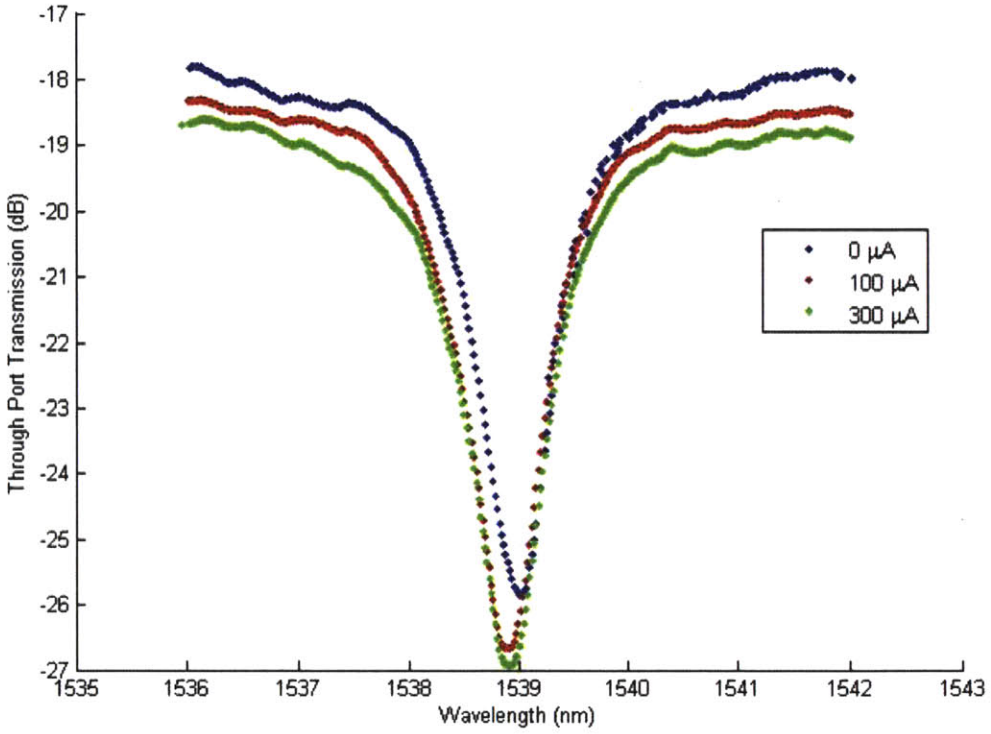

Figure 2-5: Three optical transmission scans taken at different current injections. 100 μA is enough to shift the resonance slightly, but not the full nm shift it would require for full modulation. The effect does not improve with extra current, as 300 μA performs the same. At this low frequency, the shift is dominated by the temperature's effect on the refractive index.

Wavelength (nm)	Drop Port	Fingers	Extinction Ratio (dB)	Resonance Width (nm)
1550	yes	6	5.5	1.5
1550	no	6	7.5	1.25
1550	no	4	8	1
1280	yes	6	7.5	2.5
1280	yes	6	8	2
1280	no	4	18	1
1280	no	6	26	1.5
1280	no	6	27	1.5

Table 2.1: Optical transmission data for EOS8 modulators. The drop port is the second waveguide that is coupled to the ring. The fingers are the electrical contacts to the waveguide that increase electrical current, but also increase optical loss in the ring. Extinction ratio is the depth of the resonance.

devices with drop ports. The devices with fewer fingers had narrower resonance width, because there was less optical loss in the ring. However, the devices with fewer fingers also had less current injection in the electrical measurements. From this table one can predict that the best devices for modulation would be the 1280 no drop port six finger devices.

These measurements have trends in the data, but they do not explain why certain device characteristics affect the resonances. In the next chapter I will explain the theory behind the resonances. I develop a model to explain how the resonances are generated and what can be done to improve them.

Chapter 3

Theoretical Models

In the previous Chapter I showed static data of the optical transfer characteristics of the modulators. In this chapter I show three theoretical models and how they have been used to explain the data. The three models are an analytical model, a T-matrix multiplication model and a FIMMWave model. The analytical model gives the general structure, and each of the other two models fills in some of the details. I show that these models result in matching predictions.

3.1 Analytical Model

In Chapter 1 I derived an analytical equation governing the power of light that passes through the modulator as a function of wavelength:

$$T = C\frac{t^2 - 2t\tau cos\phi + \tau^2}{1 - 2t\tau cos\phi + (t\tau)^2} \tag{3.1}$$

ϕ is the factor $2\pi L_{eff}/\lambda$, where L_{eff} is the effective length of the waveguide and λ is the wavelength. t and τ are two fitting parameters, the transmission and the loss through the ring. A coupling fitting parameter, C, is inserted in front to account for the extra loss of the fibers coupling into the waveguide on the chip.

I used Matlab's nonlinear fit function to fit transmission scans with this analytical model. This fitting process gave me values for t, τ, L_{eff} and C for each modulator

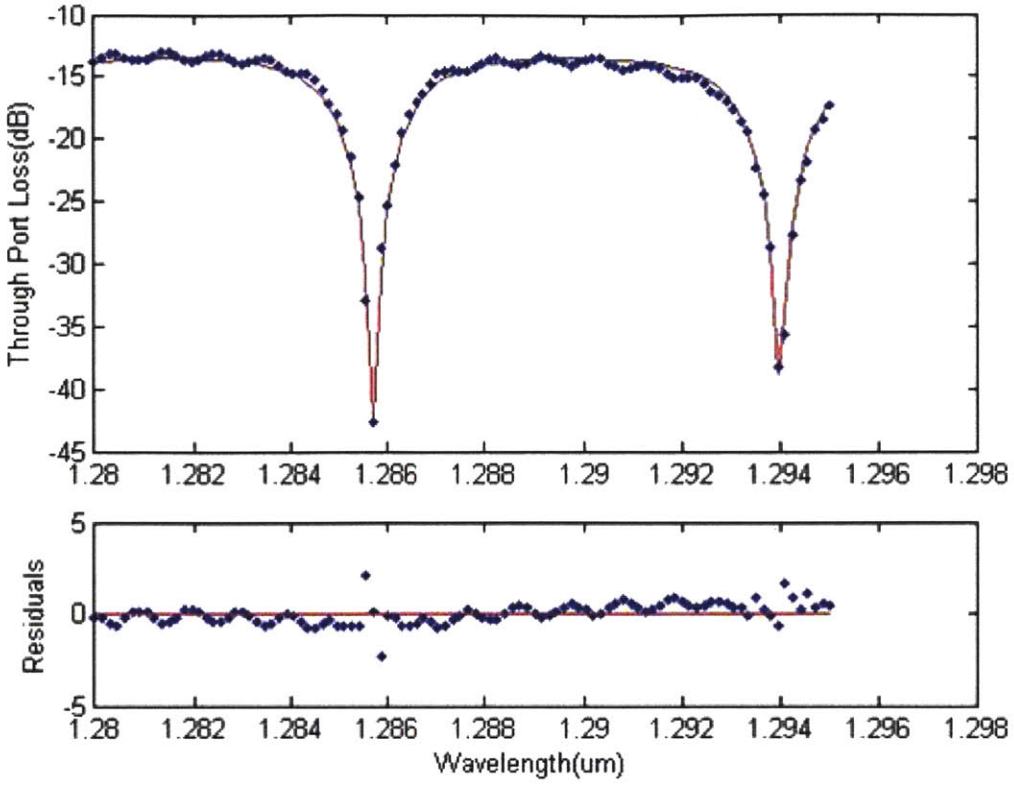

Figure 3-1: This figure shows the transmission scan of a 1280 nm modulator with no drop port. The blue dots are the experimental data and the red line is the theoretical fit. The residuals are the difference between the experimental data and the fit. They show that there is Fabry-Perot reflection between the couplers in this modulator.

tested. An example fitting is shown in Figure 3-1. The residuals in these figures closely resemble sinusoids, because there are Fabry-Perot reflections between the input and output vertical grating couplers. Each modulator was different in its amount of Fabry-Perot reflections.

This model fit the data obtained from all modulators studied. The experimentally determined parameters t, τ and L_{eff} are shown in Table 3.1. Later in this chapter I will discuss how these parameters are predicted theoretically.

Wavelength(nm)	Extinction (dB)	Res. Width (nm)	Drop?	Fingers
1550	8	1	no	4
1550	7.5	1.25	no	6
1550	5.5	1.5	yes	6
1280	27	1.5	no	6
1280	26	1.5	no	6
1280	18	1	no	4
1280	8	2	yes	6
1280	7.5	2.5	yes	6

Finger Spacing (μm)	Bus Width (nm)	t	τ	L_{eff} (μm)
2.03	674	0.88	0.76	230.8
2.03	616	0.81	0.65	232.6
2.03	590	0.79	0.51	237.9
1.185	370	0.64	0.63	200.6
1.7	370	0.64	0.62	200.6
1.7	416	0.78	0.74	200.4
1.185	364	0.61	0.39	200.5
1.7	364	0.66	0.44	200.3

Table 3.1: The design parameters of the modulators with the experimentally determined fitting parameters. The resonance width is the width on the transmission curve at 3 dB. The bus width is the width of the through waveguide at the coupling point with the ring.

3.2 Transmission Matrix Model

A small variation on this model can be made that takes into account back reflectance in the waveguides. Each component of the modulators was represented with a 2 x 2 scattering matrix that described the relationship between the inputs and the outputs of the device. An equivalent matrix, called a transmission matrix, can be created by transforming the scattering matrix. Transmision matrices can be multiplied together to get the complete transmission characteristics of the device. In modeling the devices I assumed no back reflectance in the straight waveguide and the following scattering matrix and its equivalent transmission matrix:

$$S_{through} = \begin{pmatrix} 0 & 1 \\ 1 & 0 \end{pmatrix} T_{through} = \begin{pmatrix} 1 & 0 \\ 0 & 1 \end{pmatrix} \tag{3.2}$$

For the ring waveguide I assumed there was a back reflectance R and a transmission T, yielding the following matrices:

$$S_{ring} = \begin{pmatrix} R & T \\ T & R \end{pmatrix} T_{ring} = \begin{pmatrix} \frac{1}{T} & -\frac{R}{T} \\ \frac{R}{T} & 1+\frac{R}{T} \end{pmatrix} \tag{3.3}$$

A 4x4 matrix is necessary to describe the coupling between the straight waveguide and the ring waveguide, because light travelling in both directions in both waveguides was used as the input. (This matrix is the equivalent of the matrix in Equation 1.1) This model has five fitting parameters: t, L_{eff} and C are the same as before, τ is now 1-T, and R is the back reflectance in the ring. The back reflectance is most likely caused by the boundary between different refractive indices in the fingers, but it could also be caused by roughness at the edge of the waveguides in the ring.

This formulation simplifies to the analytical model given above if R is zero, so most of the results fit equally well with each model. There were several modulators, however, for which the back reflection was a serious contribution. One of these is shown in Figure 3-2. The back reflection acounts for the dip in the middle of the transmission scan. However, most of the modulators did not have significant back

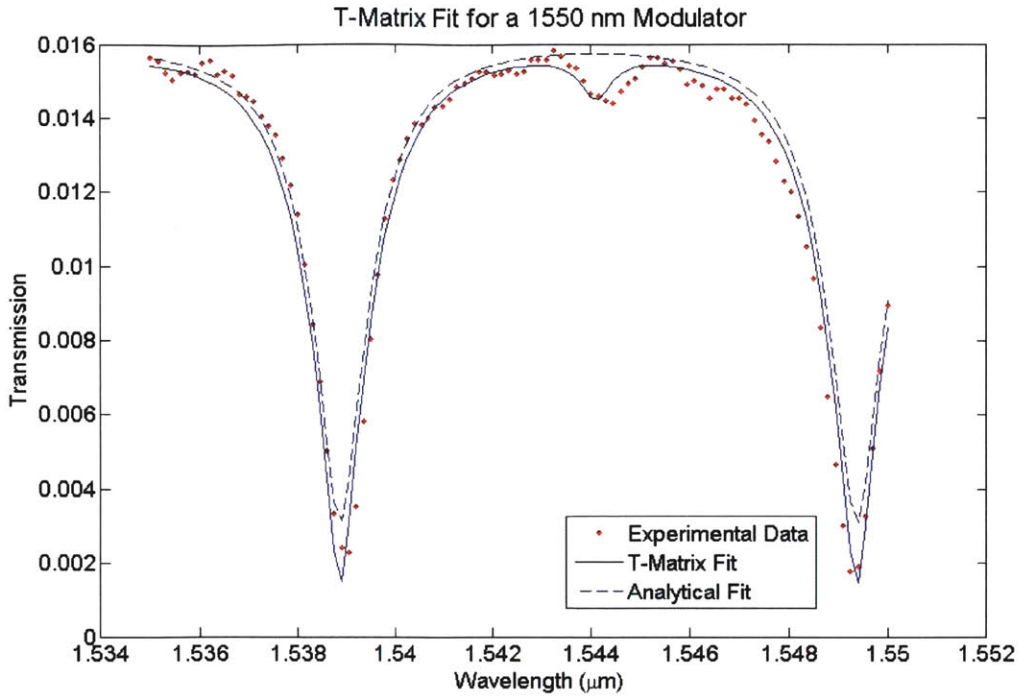

Figure 3-2: Comparison of the two different models in the case where there is a noticeable difference between them. The dip in the middle can be described by the back reflection addressed in the T-matrix model.

reflection, thus the analytical model is used for the high speed fitting described in Chapter 4.

3.3 Fimmwave Models

Another critical part of the modeling process is understanding the fitting parameters that were experimentally determined above. The transmission coefficient, t, is determined by the width of the through-waveguide and the spacing between the two coupled waveguides. A wider waveguide confines the optical mode more fully, so there is less overlap with another waveguide. Therefore, high waveguide width causes high t. Previously, Eugen Zgraggen ran Finite difference time domain (FDTD) simulations to determine the results of these different parameters [15]. The results are shown in Figure 3-3. The experimentally determined t coefficients agreed to within 10 percent with the theoretically predicted values from simulations.

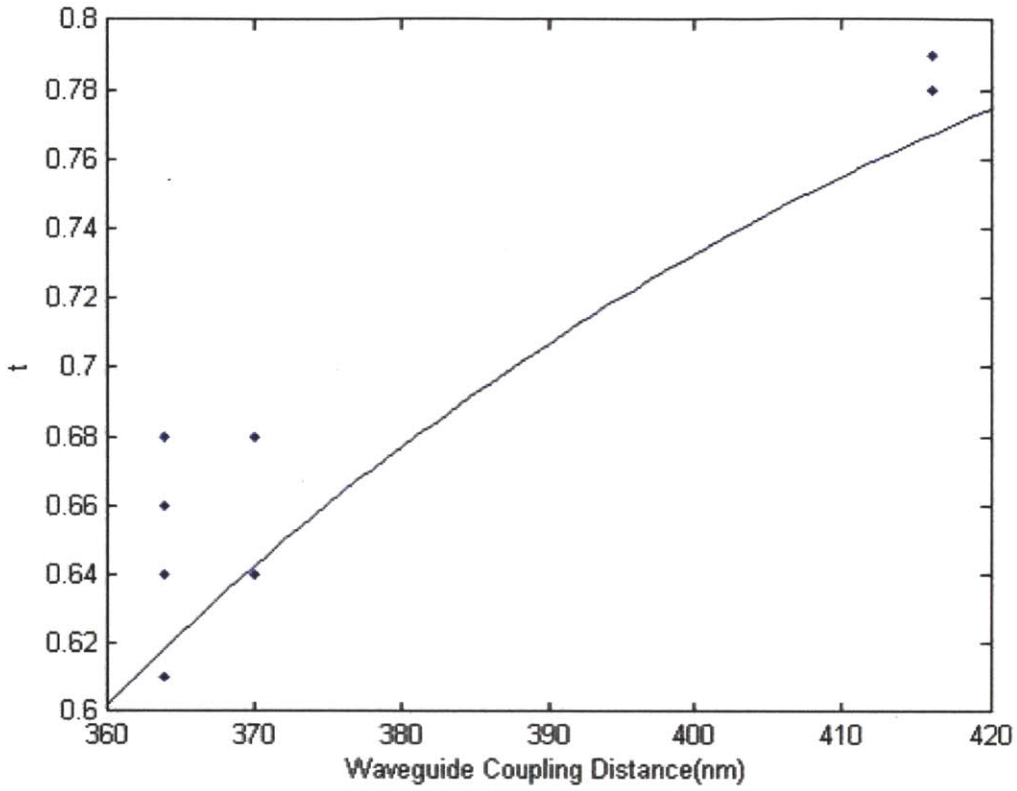

Figure 3-3: This figure shows the theoretical data (solid line) and experimental data (points) for how the transmission coefficient t varies with waveguide width. The theoretical model was made by Zgraggen. [15]

The loss coefficient, τ, is the loss within the ring. Fimmwave enables simulation and mode solving of waveguides. The spatial layouts of the materials involved are input, and FIMMWave inputs light into the waveguide material, simulating the mode confinement, optical transmission loss and back reflectance. I used a framework Zgraggen set up in Fimmwave to predict the transmission through straight waveguide sections and waveguides with finger contacts attached [15]. The loss due to regular waveguide loss was negligible compared to the loss in the contact sections. These simulations matched up to within 5 percent with the experimental data obtained for the τ parameter. The FIMMWave and FDTD models predict t and τ, which are then used in the analytical or t matrix model to predict optical transmission properties. All steps in this process fit together and with the experimental data. In the next chapter I discuss dynamic data and models.

Chapter 4

High Speed Data and Models

In this chapter I discuss the high speed operation of the modulators. I start with a discussion of the experimental setup that is used to study the modulators at high speed. I then show rise and fall time patterns and responses to pseudorandom inputs. Finally I discuss a theoretical model for the high frequency behavior of the modulators and demonstrate how the model fits with the data.

4.1 High Speed Experimental Setup and Measurement Technique

The setup for measuring high speed data was built up around the original setup for measuring static data discussed in Chapter 2. The same equipment was used to position the fibers and the stage and to electrically connect to the chip. The difference is that extra equipment was added to generate and measure the high frequency optical and electrical signals (Figure 4-1.) A clock drives an error performance analyzer at the desired frequency. The error performance analyzer outputs the electrical signal pattern: either a square wave or a pseudorandom bit sequence. This machine can also be used to measure bit error rates if the final signal is input into the machine, which will be important later for testing the effectiveness of the complete optical link. The electrical pattern from the error performance analyzer is passed through a

modulator driver and an attenuator to produce a signal with the appropriate shape and amplitude for driving the on-chip modulators. The signal must be attenuated so that it is not so powerful that it destroys the devices. Using a bias tee, a constant (DC) voltage is added to the signal through an inductor to change the bias point. Finally this signal is input to a modulator using a three tip GSG (ground, signal, ground) probe.

The output optical signal is coupled into a fiber as before, but now it is fed into an EDFA (erbium doped fiber amplifier). The EDFA amplifies the signal, but it also introduces noise at other light frequencies, so the light is passed through a tunable filter to select only the target wavelength. Finally the signal is passed to a digital communications analyzer, which behaves a lot like an optical oscilloscope. Optical power is displayed as a function of time, and many periods of data are overlayed onto the same plot, producing an eye-diagram in the case of a pseudorandom bit pattern. The data from this machine are read into the computer via GPIB.

As the modulator heats up, the resonance frequency of the modulator shifts. This means that it is often necessary to shift the wavelength of the input laser to optimize its location on the wavelength transmission scan. To take a transmission scan of the modulator without changing the setup, a broadband light source is coupled with the input light using a 90/10 splitter. The output is split using a 90/10 splitter, with 10 percent going to an optical spectrum analyzer, a device that measures the power at each frequency. When the broadband light source is turned on, the optical spectrum analyzer takes a qualitative transmission scan that includes a spike at the laser wavelength. This feature is very useful in the experiment. The first test of this setup was the square wave response discussed in the next section.

4.2 Rise and Fall Pattern Responses

The first step in determining the high speed response of the system was determining the response to a simple square wave pattern. This pattern enabled a study of the rise and fall patterns as the modulator was turned on and off. I chose to quantify the

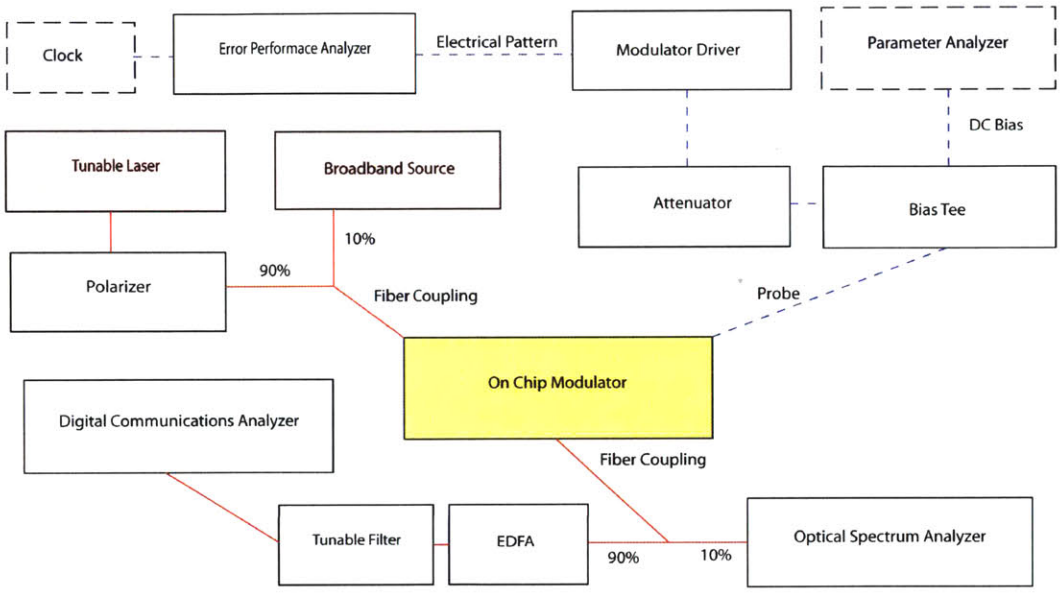

Figure 4-1: Extra equipment for generating and measuring high speed signals. Electrical signals and sources are colored blue with dashed lines and photonic signals and sources are colored red with solid lines. The broadband source is used to determine the current transmission scan, and it is not turned on during pattern response experiments.

rise time as the time between 10 percent and 90 percent power and the fall time as the time between 90 percent and 10 percent power. The main mechanisms for rise and fall time are carrier injection and carrier recombination. Carrier injection occurs during the transition to an electrical "1" or high voltage as electrons and holes from the n and p regions at the side of the waveguide drift into the waveguide. Carrier recombination occurs during the transition to an electrical "0" or low voltage as the electrons and holes in the waveguide recombine. Depending upon which side of the resonance the laser was on, the optical states were either the same or the opposite of the electrical states.

The rise and fall times and amplitude of modulation of the modulators depended on many different factors including wavelength, temperature, frequency, electrical bias point and size of voltage signal applied. The wavelength of the input laser light had a large effect, because only the places on the transmission scan with steeply sloped power have a large difference in power when a current is injected. The wavelength dependence of the amplitude of modulation (Figure 4-2a) demonstrated that one side of the resonance was more effective than the other. This can be explained by current shifting the critical coupling condition. Current changes the optical loss in the ring τ, and hence pushes the ring closer or farther from critical coupling. Because this particular ring is undercoupled, the change in τ shifts the modulator towards critical coupling, deepening the resonance and making the higher wavelength side of the resonance more effective (Figure 4-2b.)

Temperature also had a large effect on the modulation. When current was run through the modulators for long periods of time heat was dissipated, and the temperature rose, shifting the refractive index and the optical absorption of the silicon waveguide. Higher temperature resulted in a shifted shallower resonance and a corresponding decreases in amplitude. This effect was evident both from looking at the broadband transmission spectrum and from the pattern responses shown in Figure 4-3.

Electrical bias point and the attenuation that determines the size of the voltage signal were both adjusted so as to optimize the amplitude of the modulation. Gen-

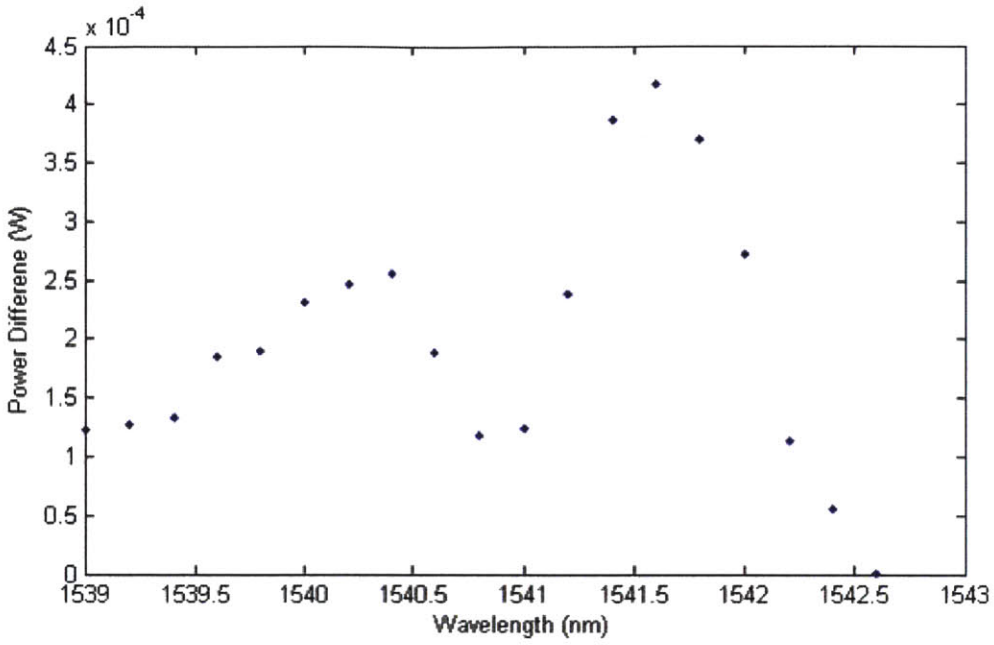

(a)

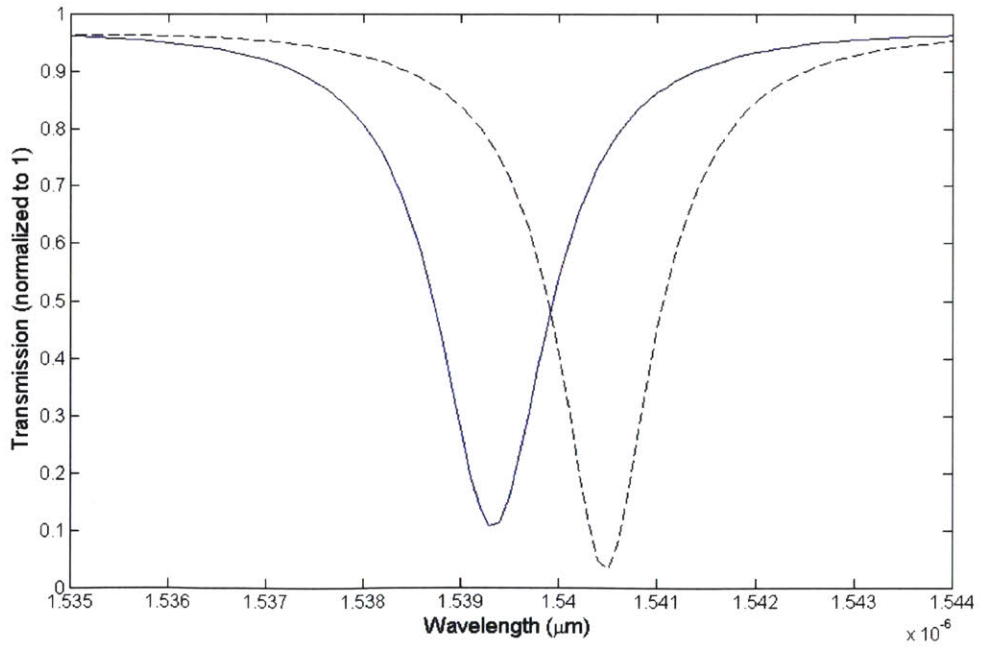

(b)

Figure 4-2: (a) Dependence of the modulation amplitude on the wavelength. The modulation is larger on the higher wavelength side of the resonance. This can be explained by a difference in coupling. (b) Theoretical model for the relationship between transmission scan and applied current. The solid line is no current, and the dotted line is with current. The amplitude is the difference between these two curves and it is uneven, explaining the experimental results. These data were taken using a 1550 nm slab modulator from the EOS8 run.

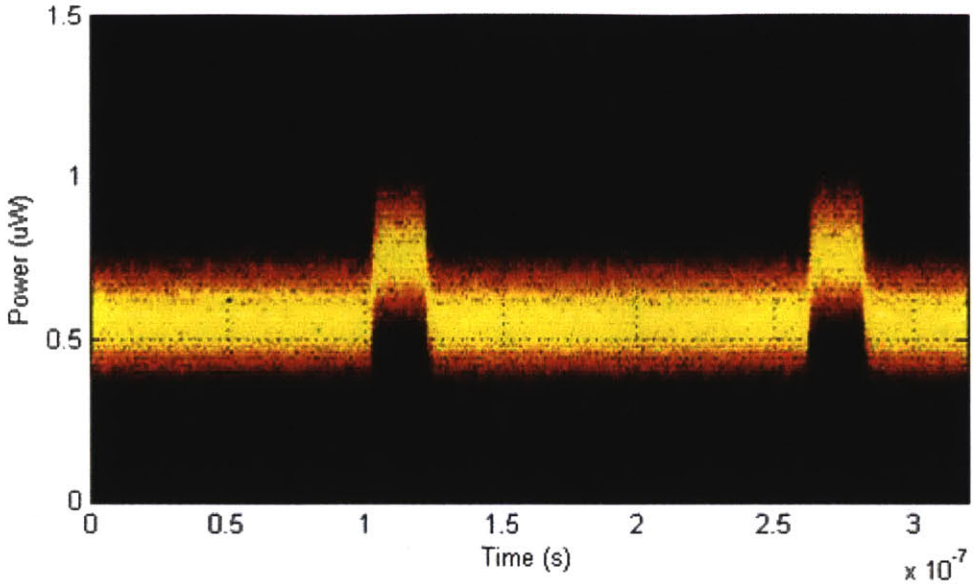

(a) 28 0's and 4 1's

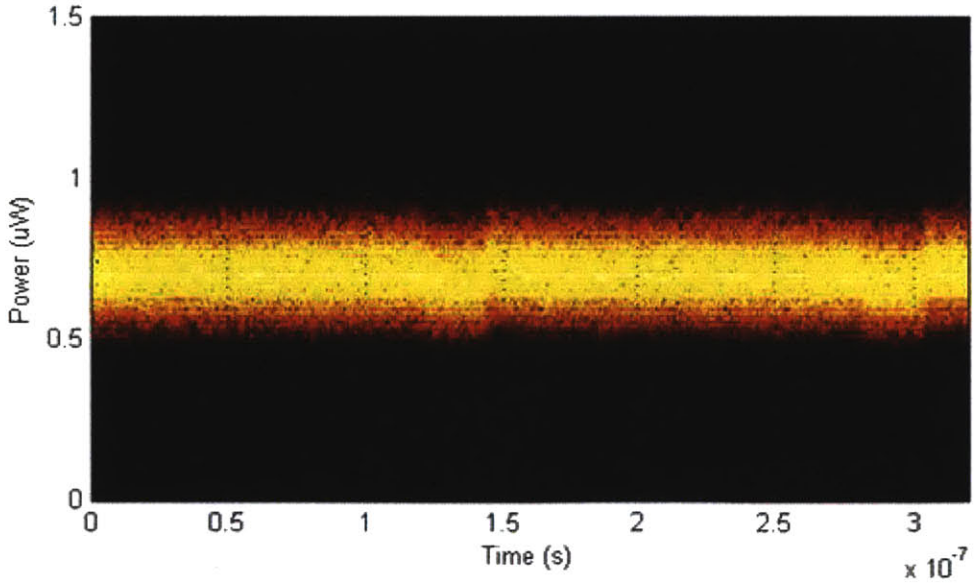

(b) 28 1's and 4 0's

Figure 4-3: Responses to two different electrical pattern inputs. If the temperature rises during a long period of current injection(1's), the resonance is shifted, and there is almost no modulation when the current is switched off, as in 4-3b. However a long string of no current(0's) has no effect on the temperature, so there is still modulation when the current is switched on, as in 4-3a. These data were taken using a 1550 nm rib modulator from the EOS8 run.

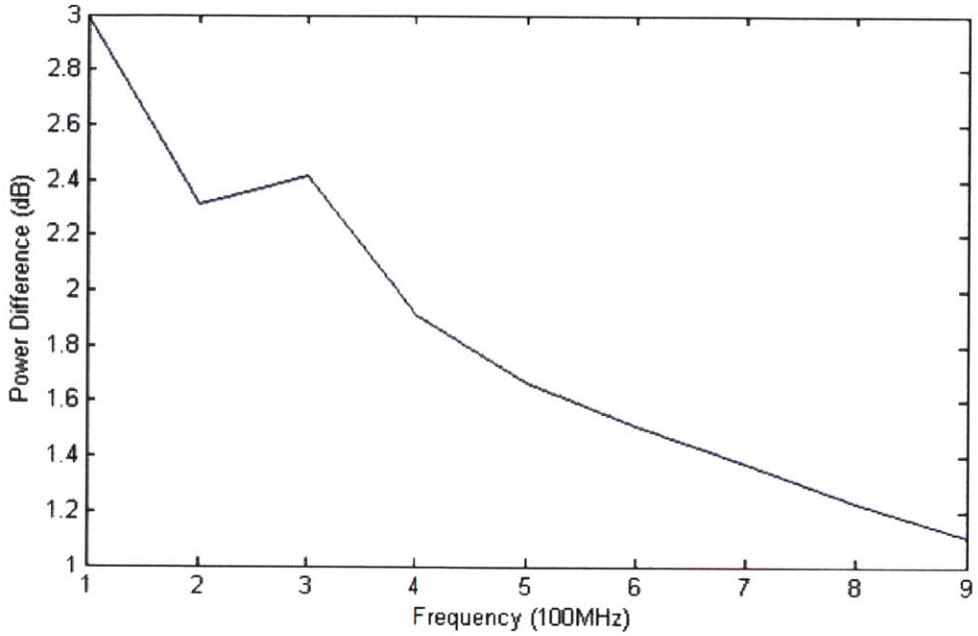

Figure 4-4: Amplitude dependence on frequency. At higher frequencies the modulator does not have time to reach its full carrier concentration, so the amplitude is decreased. These data were taken using a 1550 nm slab modulator from the EOS8 run.

erally a bias voltage of around 0.5 Volts was used. The frequency of the modulation also affected the amplitude (Figure 4-4), because if the time between rise and fall was too short the modulator did not complete the transition. The effect of frequency is especially important, because one of the goals is to develop modulators that can work in the 5-10 GHz range. Another goal is to have the modulators operate with any arbitrary pattern of input. The response to pseudorandom bit sequences is described in the next section.

4.3 Pseudorandom Bit Sequences

A pseudorandom bit sequence (PRBS) was useful for testing how a modulator would respond to a real stream of data. The length of time between rise and fall transitions was no longer fixed, so there was a distribution of amplitudes and rise and fall times depending upon the particular pattern. In our system, individual sets of data from

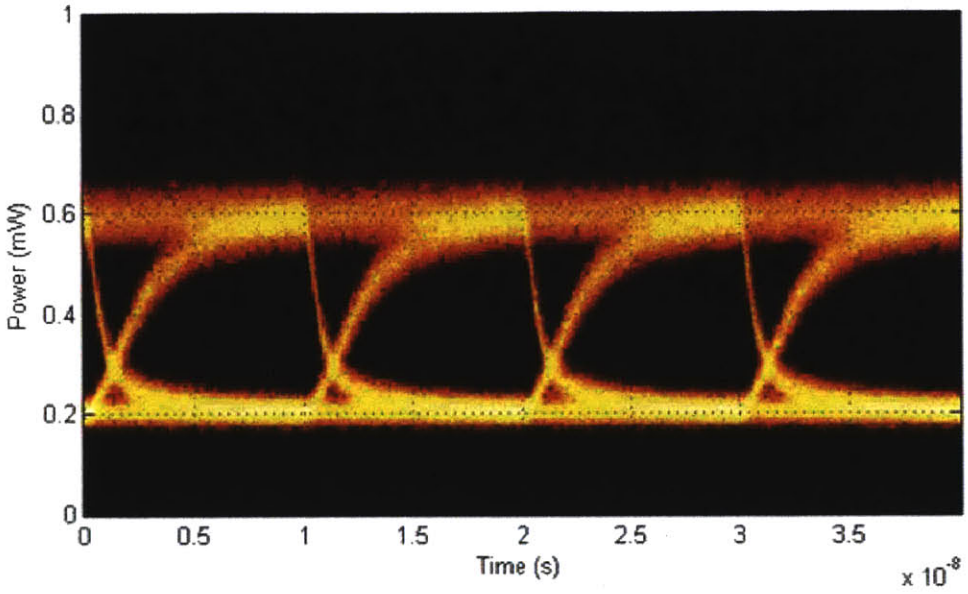

Figure 4-5: An eye-diagram taken at a frequency of 100 MHz. The lighter colors represent a higher density of points falling in that region. The large gap in the middle of each period is the "eye", and it is crucial that this space be empty enough to distinguish between the on and off state. These data were taken using a 1550 nm slab modulator from the EOS8 run.

each period were overlayed on top of each other to make an "eye diagram". An example is shown in Figure 4-5.

As was discussed above, at higher frequency the amplitude of modulation decreased. This same effect was evident with the PRBS pattern input. Above a frequency of 600 MHz it was hard to distinguish an "eye" (the space between a "1" and a "0" in the center of the diagram,) as the on and off states of the modulator began to blend together. There were also two different rises, because if the modulator did not have time to fully reach the "1" state it rose sooner. There were two lines corresponding to a single "1" followed by a "0" and multiple "1's" followed by a "0". These effects can be seen in Figure 4-6.

One method of improving the performance of the modulator is to use a technique called pre-emphasis. Pre-emphasis involves putting in a pattern that starts each "1" with a higher voltage, then comes down to the normal voltage. With this technique the modulator turns on faster, so there is less rise time. Using pre-emphasis should

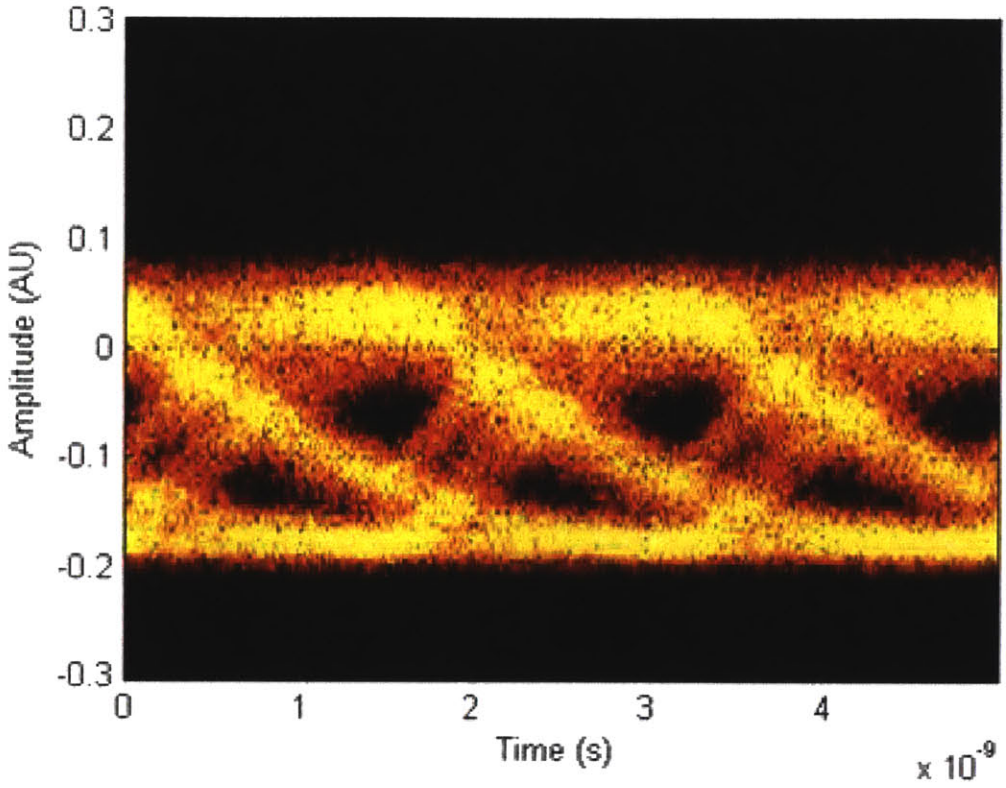

Figure 4-6: An eye-diagram taken at a frequency of 500 MHz. The wavelength of the laser is on the high wavelength side of the resonance, so injecting current lowers the optical power. There are two different rise times, because if the modulator has not had time to inject enough carriers, the carriers recombine sooner. These data were taken with a 1550 nm rib modulator from the EOS8 run.

increase both the amplitude and the maximum frequency at which the modulators can be driven. This technique has been implemented in some of the driver circuits for the modulators designed by other members of our collaboration.

4.4 Dynamic Model

In this section I describe a model I have developed to explain the high-speed data collected. This model was developed around four main equations that generally apply to carrier injection modulators. (Both the slab and rib modulators fall into this category.) The first of these equations is the dynamic equation governing the free carrier concentration, N, within the waveguide.

$$\frac{dN}{dt} = \frac{I}{qV} - \frac{N}{\tau_n} \tag{4.1}$$

I is the current through the device, q is the elementary charge, V is the volume of the device, and τ_n is the carrier lifetime. The first term models the current injection of carriers and the second term models the carrier recombination.

The second equation involves the temperature, T, of the device as heat is dissipated by the current.

$$\frac{dT}{dt} = \frac{I^2 R}{c\rho V} - \frac{T - T_{room}}{R_{th}} \tag{4.2}$$

R is the resistance when the diode is forward biased, c is the specific heat, ρ is the density, V is the volume of the device, and R_{th} is a constant representing how heat is dissipated away from the device's contact region.

The third and fourth equations determine how the refractive index, n, and absorption coefficient, α, of silicon depend on the carrier concentration and temperature. These equations were empirically found by Soref and Jellison [14, 16].

$$\Delta n = -10^{-22.2}\Delta N^{1.05} - 10^{-17.56}\Delta N^{0.805} + 1.85 * 10^{-4}\Delta T \tag{4.3}$$

$$\Delta\alpha = 10^{-17.7}\Delta N + 10^{-17.8}\Delta N + 0.5\Delta T^{0.0058} \tag{4.4}$$

Parameter	Value
q	1.602 x 10^{-19} C
V	4 x $10^{-14} m^3$
τ_n	10^{-6} s
R	0.0062 Ω
c	2.33 J/Kkg
ρ	7.1 x 10^5 gcm^{-3}
R_{th}	$10^{-6} s$

Table 4.1: These are the parameters used in Equations 4-1 to 4-4.

ΔN is the change in carrier concentration and ΔT is the change in temperature. Together with the models developed in Chapter 3, these equations provide a framework for modeling the optical transmission through the modulators in response to an input current pattern.

I used Matlab to run an eye diagram simulation using these equations as the basis. The input was a pseudorandom arrangement of a square wave pattern in current, I. First Equations 4.1 and 4.2 were solved using a Matlab ODE solver. The results were used to calculate the shift in refractive index and optical absorption. Finally these shifts were used to calculate the output optical power using the analytical equation from Chapter 3. R_{th} was set to match experimental data as well as possible, and V was estimated from the designs. The other constants are well established material properties (Table 4.1). The results are shown in Figure 4-7.

The model can also be used to demonstrate some of the properties mentioned before. For example: the double line pattern occurs in simulation at higher frequencies (Figure 4-8.) Injection pattern can also be changed in the simulation using pre-emphasis, as will be discussed in more detail in the next Chapter. In the next section I summarize the conclusions from my experiments and models, and I describe improvements that can be made to the modulators to increase performance.

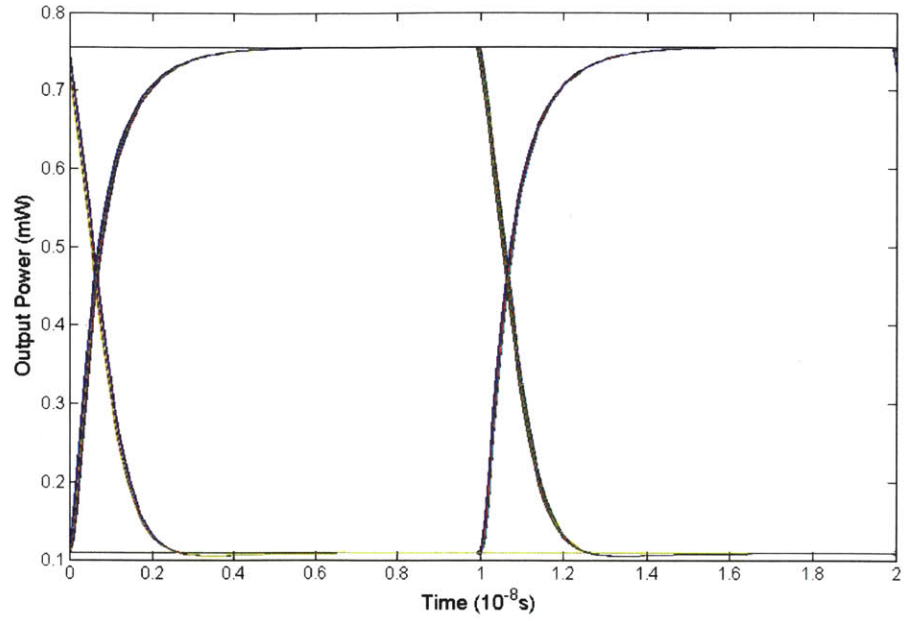

(a)

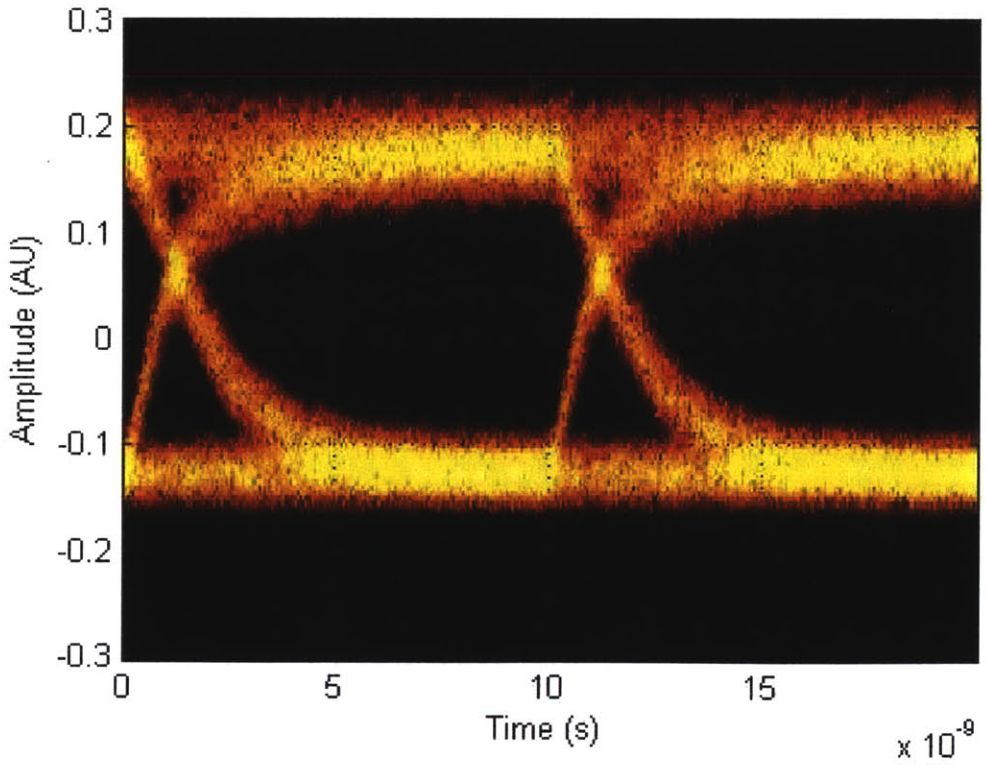

(b)

Figure 4-7: This figure shows the results of the model on a 1550 nm modulator (4-7a) and experimental results (4-7b). The two match each other well.

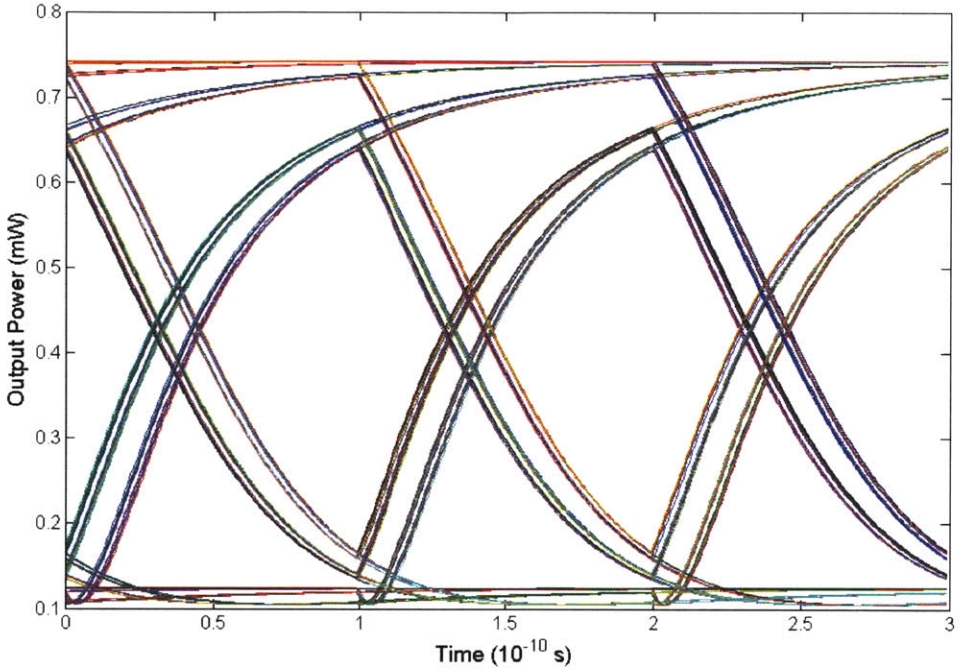

Figure 4-8: This figure demonstrates that double lines appear in simulation at high frequencies. In this case there is a double line on both the injection and the recombination curve, because both the rise time and the fall time are longer than the period.

Chapter 5

Suggested Improvements

One of the main goals of this thesis is to identify and understand the physical properties of the modulators. With this data it is possible to suggest improvements, so that future runs can produce better modulators. In this Chapter I suggest three improvements and then provide some concluding remarks about the thesis.

5.1 Changing Coupling Distances

As was mentioned in Chapter 1, modulators with t = τ perform the best. Most of the modulators are undercoupled, and this condition is not met. The coefficient of transmission, t, is easier to control than the loss in the ring, τ, because the loss in the ring is necessary to make the electrical injection possible. t can be changed by changing the distance between the two waveguides or by changing their widths. This coupling was modeled by Eugen Zgraggen as discussed in Chapter 3 [15]. I therefore suggest changing the waveguide widths in the coupling regions to better match the loss, τ. This is especially important in devices with drop ports, because all of the drop port devices had a large difference between t and τ.

The waveguides in all of the 1550 nm devices and in the 1280 nm devices with drop ports should be narrower to decrease t. For the drop port devices this corresponds to a change in waveguide width from about 360 nm to 300 nm. Producing modulators with critical coupling could increase the extinction ratio by as much as 20 dB. The t

Wavelength(nm)	Drop?	Bus Width (nm)	t	τ	Extinction Ratio (dB)
1550	no	590	0.78	0.65	12.5
1550	no	674	0.88	0.76	8
1550	no	616	0.81	0.65	7.5
1550	yes	590	0.79	0.51	5.5
1280	no	370	0.64	0.63	27
1280	no	370	0.64	0.62	26
1280	no	416	0.78	0.74	18
1280	yes	364	0.61	0.39	8
1280	yes	364	0.66	0.44	7.5

Table 5.1: This table shows the bus widths of the modulators with the experimentally determined fitting parameters. The bus width is the width of the through waveguide at the coupling point with the ring. The first entry is from the new run EOS12 and all the other entries are from the older run EOS8.

coefficients and waveguide widths are given again in Table 5.1. These predictions use extrapolation, however, so full simulation would provide more acurate predictions.

The next run, EOS12, has some devices on it with different bus widths. Not all of the devices have been measured yet, but the 1550 nm device with a narrower bus width performed better, because t was closer to τ. However, an even narrower bus width will be required to reach the critical coupling condition.

5.2 Pre-emphasis

There are also methods of improving the dynamic response of the modulators. One of these methods is to inject extra current into the modulator during its rise phase to make its rise phase faster. As the limiting time at high frequency was the injection time (not the recombination time), pre-emphasis should increase the maximum frequency of operation for the modulators. I ran a simulation in which pre-emphasis for one twentieth of a period at double the injection decreased the injection time to less than half of the normal level (Figure 5-1). This is an important step towards reaching the goal of modulation at 5 Gbit/s. Other people in our collaboration have driver circuits on the chip that should be able to perform the pre-emphasis.

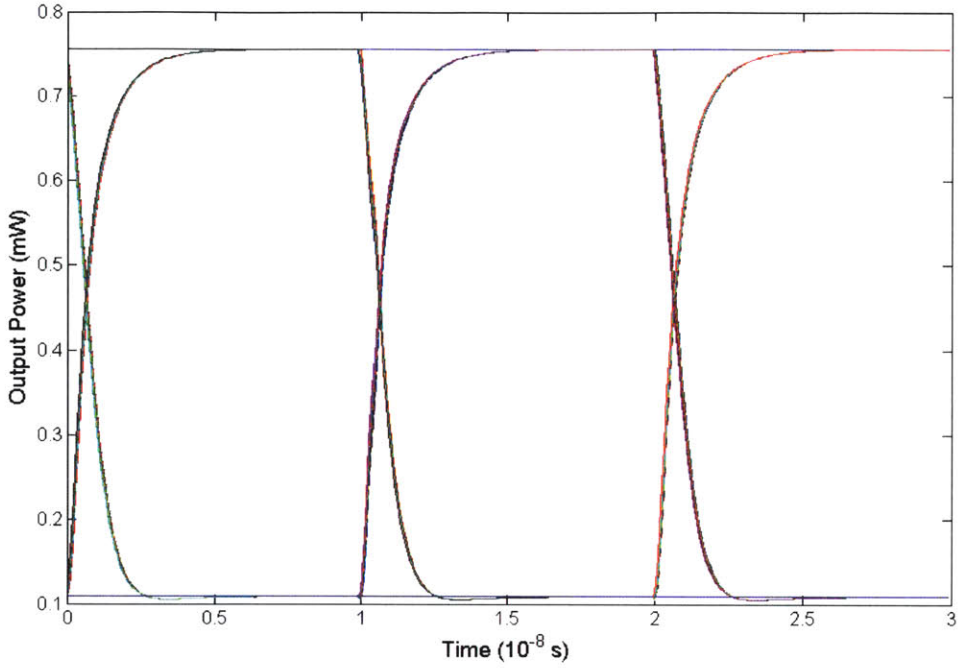

(a)

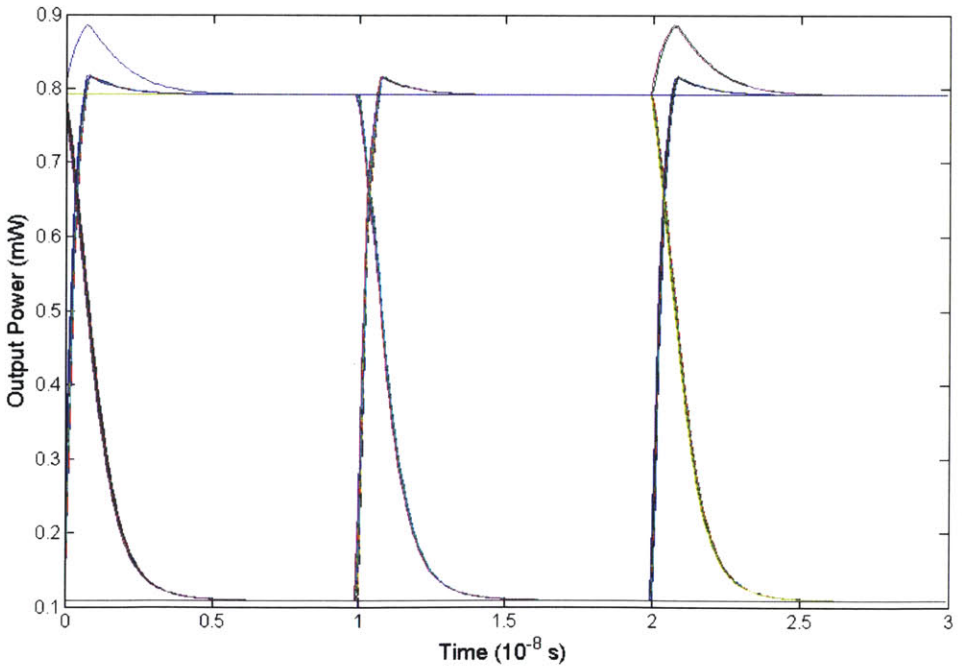

(b)

Figure 5-1: Comparison of simulated modulation with (5-1b) and without (5-1a) pre-emphasis. The pre-emphasis lasted for 0.5 ns at an additional current of 60 mA(double current).

5.3 Slab vs. Rib modulators

This thesis adresses two different types of ring resonator modulators: slab and rib modulators. Although the two types have similar overall structure, the waveguide structure is different. In general, the rib modulator structures had deeper and narrower resonances. However, the injection time for the rib modulators was longer, because the contact are farther from the waveguide. Therefore the rib modulators operated at a slower rate than the slab modulators. The pre-emphasis technique should improve the injection time for both devices, so it is likely that the rib modulator devices will work better overall.

5.4 Conclusion

In this thesis I have studied the physics of how modulators operate. Eugen Zgraggen and Jason Orcutt designed devices to be close to critical coupling[15, 3], and I have tested the physical properties of these devices. I started by constructing a general optical testing station capable of measuring the optical transmission signature and electrical IV characteristics of any device. I then measured the optical transmission spectrums and IV curves of modulators from three runs (EOS2, EOS8 and EOS10) to compare them and find the best devices. I developed three models: an analytical model, a transmission matrix model and an optical simulation model to explain three different aspects of the modulators. These models enabled me to compare predictions of operation with the actual devices themselves.

In the next step I went beyond the predictions of the design simulations into the high frequency domain. I measured the optical response to electrical signals at high frequency and modeled this using rate equations. Finally, I have suggested several improvements for the modulators, and demonstrated that these can lead to better performance.

More runs will happen and the chips will continue to develop with better devices each time. Eventually we may produce optical interconnects that are a good alter-

native to the electrical interconnects used today, leading to faster and more energy efficient computers.

Bibliography

[1] D.A.B. Miller. Rationale and challenges for optical interconnects to electronic chips. *Proceedings of the IEEE*, 88(6):728–749, June 2000.

[2] M. Haurylau et. al. On-chip optical interconnect roadmap: challenges and critical directions. *IEEE International Conference on Group IV Photonics, 2005*, pages 17–19, September 2005.

[3] Jason S. Orcutt. *Monolithic Electronic-Photonic Integration in State-of-the-Art CMOS Processes.* PhD thesis, MIT, February 2012.

[4] Frank O'Mahony et. al. The future of electrical I/O for microprocessors. In *2009 International Symposium on VLSI Design, Automation and Test*, pages 31–34. IEEE, April 2009.

[5] Jason S. Orcutt et. al. Nanophotonic integration in state-of-the-art CMOS foundries. *Optics Express*, 19(3):2335–2346, January 2011.

[6] S. J. Spector et. al. CMOS-compatible dual-output silicon modulator for analog signal processing. *Optics Express*, 16(15):11027–11031, July 2008.

[7] William M. Green, Michael J. Rooks, Lidija Sekaric, and Yurii A. Vlasov. Ultra-compact, low RF power, 10 Gb/s silicon Mach-Zehnder modulator. *Optics Express*, 15(25):17106–17113, December 2007.

[8] Sasikanth Manipatruni, Kyle Preston, Long Chen, and Michal Lipson. Ultra-low voltage, ultra-small mode volume silicon microring modulator. *Optics Express*, 18(17):18235–18242, August 2010.

[9] Xuezhe Zheng et. al. Ultra-low-energy all-CMOS modulator integrated with driver. *Optics Express*, 18(3):3059–3070, January 2010.

[10] Qianfan Xu et. al. 125 Gbit/s carrier-injection-based silicon micro-ring silicon modulators. *Optics Express*, 15(2):430–436, January 2007.

[11] C. Gunn. CMOS Photonics for High-Speed Interconnects. *IEEE Micro*, 26(2):58–66, March 2006.

[12] Michael R. Watts et al. Vertical junction silicon microdisk modulators and switches. *Optics Express*, 19(22):21989–22003, October 2011.

[13] Jan Niehusmann et. al. Ultrahigh-quality-factor silicon-on-insulator microring resonator. *Optics Letters*, 29(24):2861–2863, December 2004.

[14] R. Soref and B. Bennett. Electrooptical effects in silicon. *IEEE Journal of Quantum Electronics*, 23(1):123–129, January 1987.

[15] Eugen Zgraggen. *Design and Optimization of a Silicon Electro-Optic Modulator.* PhD thesis, ETH Zurich, September 2009.

[16] G. E. Jellison. Optical absorption coefficient of silicon at 1.152 μm at elevated temperatures. *Applied Physics Letters*, 41(7):594–596, October 1982.